Wetting on a spherical wall: Influence of liquid-gas interfacial properties

Andreas Nold*
Center of Smart Interfaces, TU Darmstadt, Petersenstrasse 32, D-64287 Darmstadt, Germany and
Department of Chemical Engineering, Imperial College London, London SW7 2AZ, United Kingdom

Alexandr Malijevský†
E. Hála Laboratory of Thermodynamics, Institute of Chemical Process Fundamentals of ASCR, CZ-16502 Prague 6, Czech Republic and
Department of Physical Chemistry, Institute of Chemical Technology, Prague, CZ-166 28 Praha 6, Czech Republic

Serafim Kalliadasis‡
Department of Chemical Engineering, Imperial College London, London SW7 2AZ, United Kingdom
(Received 29 March 2011; published 22 August 2011)

We study the equilibrium of a liquid film on an attractive spherical substrate for an intermolecular interaction model exhibiting both fluid-fluid and fluid-wall long-range forces. We first reexamine the wetting properties of the model in the zero-curvature limit, i.e., for a planar wall, using an effective interfacial Hamiltonian approach in the framework of the well known sharp-kink approximation (SKA). We obtain very good agreement with a mean-field density functional theory (DFT), fully justifying the use of SKA in this limit. We then turn our attention to substrates of finite curvature and appropriately modify the so-called soft-interface approximation (SIA) originally formulated by Napiórkowski and Dietrich [Phys. Rev. B **34**, 6469 (1986)] for critical wetting on a planar wall. A detailed asymptotic analysis of SIA confirms the SKA functional form for the film growth. However, it turns out that the agreement between SKA and our DFT is only qualitative. We then show that the quantitative discrepancy between the two is due to the overestimation of the liquid-gas surface tension within SKA. On the other hand, by relaxing the assumption of a sharp interface, with, e.g., a simple "smoothing" of the density profile there, markedly improves the predictive capability of the theory, making it quantitative and showing that the liquid-gas surface tension plays a crucial role when describing wetting on a curved substrate. In addition, we show that in contrast to SKA, SIA predicts the expected mean-field critical exponent of the liquid-gas surface tension.

DOI: 10.1103/PhysRevE.84.021603 PACS number(s): 68.08.Bc, 05.20.Jj, 71.15.Mb, 05.70.Np

I. INTRODUCTION

The behavior of fluids in confined geometries, in particular, in the vicinity of solid substrates, and associated wetting phenomena are of paramount significance in numerous technological applications and natural phenomena. Wetting is also central in several fields, from engineering and materials science to chemistry and biology. As a consequence, it has received considerable attention, both experimentally and theoretically, for several decades. Detailed and comprehensive reviews are given in Refs. [1–4].

Once a substrate (e.g., a solid wall) is brought into contact with a gas, the substrate-fluid attractive forces cause adsorption of some of the fluid molecules on the substrate surface, such that at least a microscopically thin liquid film forms on the surface. The interplay between the fluid-fluid interaction (cohesion) and the fluid-wall interaction (adhesion) then determines a particular wetting state of the system. This state can be quantified by the contact angle at which the liquid-gas interface meets the substrate. If the contact angle is nonzero, i.e., a spherical cap of the liquid is formed on the substrate, the surface is called partially wet. In the regime of partial wetting, the cap is surrounded by a thin layer of adsorbed fluid which is of molecular dimension. Upon approaching the critical temperature, the contact angle continuously decreases and eventually vanishes. Beyond this wetting temperature one speaks of complete wetting and the film thickness becomes of macroscopic dimension. The transition between the two regimes can be qualitatively distinguished by the rate of disappearance of the contact angle, which is discontinuous in the case of a first-order transition or continuous for critical wetting.

From a theoretical point of view, it is much more convenient to take the adsorbed film thickness ℓ, rather than the contact angle, as an order parameter for wetting transitions and related phenomena. An interfacial Hamiltonian is then minimized with respect to ℓ as is typically the case with the (mesoscopic) Landau-type field theories and (microscopic) density functional theory (DFT)—where ℓ can be easily determined from the Gibbs adsorption, a direct output of DFT.

In this study, we examine the wetting properties of a simple fluid in contact with a spherical attractive wall by using an intermolecular interaction model with fluid-fluid and fluid-wall long-range forces. The curved geometry of the system prohibits a macroscopic growth of the adsorbed layer (and thus complete wetting), since the free-energy contribution due to the liquid-gas interface increases with the film thickness ℓ, and thus for a given radius of a spherical substrate there must be a maximum finite value of ℓ [1,5,6]. For the mesoscopic approaches, the radius of the wall R is a new field variable that

*andreas.nold09@imperial.ac.uk
†a.malijevsky@imperial.ac.uk
‡s.kalliadasis@imperial.ac.uk

introduces one additional ℓ-dependent term to the effective interface Hamiltonian of the system, compared to the planar geometry, where the only ℓ-dependent term is the binding potential between the wall-liquid and liquid-gas interfaces. Furthermore, for a fluid model exhibiting a gas-liquid phase transition, such as ours, it has been found that two regimes of the interfacial behavior should be distinguished: $R > R_c$, in which case the surface tension can be expanded in integer powers of R^{-1} and $R < R_c$, where the interfacial quantities exhibit a nonanalytic behavior [7]. Moreover, for an intermolecular interaction model with fluid-fluid long-range interactions, there is an additional $R^{-2} \ln R$ contribution to the surface tension in the $R > R_c$ regime [8]. These striking observations actually challenge all curvature expansion approaches. In addition, a certain equivalence between a system of a saturated fluid on a spherical wall and a system of an unsaturated fluid on a planar wall above the wetting temperature has been found [5,8]. Somewhat surprisingly, DFT computations confirmed this correspondence at the level of the density profiles down to unexpectedly small radii of the wall [8].

Most of these conjectures follow from the so-called sharp-kink approximation (SKA) [1], based on a simple piecewise constant approximation of a one-body density distribution of the fluid, i.e., a coarse-grained approach providing a link between mesoscopic Hamiltonian theories and microscopic DFT. The simple mathematical form of SKA has motivated many theoretical investigations of wetting phenomena, as it makes them analytically tractable. At the same time, SKA appears to capture much of the underlying fundamental physics for planar substrates (often in conjugation with exact statistical mechanical sum rules [9]).

However, as we show in this work, SKA is only qualitative for spherical substrates, even though the functional form of the film growth can still be successfully inferred from the theory [8]. We attribute this to the particular approximation of the liquid-gas interface adapted by SKA. In particular, since the ℓ-dependent contribution to the interface Hamiltonian due to the curvature is proportional to the liquid-gas surface tension, the latter plays an important role compared to the planar geometry.

More specifically, the curved geometry induces a Laplace pressure whose value depends on both film thickness and surface tension, and so the two quantities are now coupled, in contrast with the planar geometry where a parallel shift of the liquid-gas dividing surface does not influence the surface contribution to the free energy of the system. We further employ an alternative coarse-grained approach, a modification of the one originally proposed by Napiórkowski and Dietrich [10] for the planar geometry, which replaces the jump in the density profile at the liquid-gas interface of SKA by a continuous function restricted by several reasonable constraints. We show that in this "soft-interface approximation" (SIA) the leading curvature correction to the liquid-gas surface tension is $O(R^{-1})$, rather than $O(R^{-2} \ln R)$, in line with the Tolman theory. Once a particular approximation for the liquid-gas interface is taken, the corresponding Tolman length can be easily determined. Apart from this, we find that the finite width of the liquid-gas interface significantly improves the prediction of the corresponding surface tension when compared with the microscopic DFT computations, which consequently markedly improves the estimation of the film thickness in a spherical geometry.

In Sec. II we describe our microscopic model and the corresponding DFT formalism. In Sec. III we present results of wetting phenomena on a planar wall obtained from our DFT based on a continuation scheme that allows us to trace metastable and unstable solutions. The results are compared with the analytical prediction as given by a minimization of the interface Hamiltonian based on SKA. We also make a connection between the two approaches by introducing the microscopic model into the interfacial Hamiltonian. In Sec. IV we turn our attention to the main part of our study, a thin liquid film on a spherical wall. We show that SKA does not account for a quantitative description of the liquid-gas surface tension which plays a significant role when the substrate geometry is curved. We then introduce SIA and present an asymptotic analysis with our approach. Comparison with DFT computations reveals a substantial improvement of the resulting interface Hamiltonian, even for very simple approximations of the density distribution at the liquid-vapor interface, indicating the significance of a nonzero width of the interface. We conclude in Sec. V with a summary of our results and discussion. Appendix A describes the continuation method we developed for the numerical solution of DFT. In Appendix B we show derivations of the surface tension and the binding potential for both a planar and a spherical geometry within SKA. Finally, Appendix C shows derivations of the above quantities, including Tolman's length, using SIA.

II. DFT

A. General formalism

DFT is based on Mermin's proof [11] that the free energy of an inhomogeneous system at equilibrium can be expressed as a functional of an ensemble averaged one-body density, $\rho(\mathbf{r})$ (see, e.g., Ref. [12] for more details). Thus, the free-energy functional $\mathcal{F}[\rho]$ contains all the equilibrium physics of the system under consideration. Clearly, for a three-dimensional fluid model one has to resort to an approximative functional. Here we adopt a simple but rather well established local density approximation,

$$\mathcal{F}[\rho] = \int f_{\mathrm{HS}}[\rho(\mathbf{r})]\rho(\mathbf{r})\,d\mathbf{r} + \frac{1}{2}\iint \rho(\mathbf{r})\rho(\mathbf{r}')\phi(|\mathbf{r}-\mathbf{r}'|)\,d\mathbf{r}'\,d\mathbf{r}, \tag{1}$$

where $f_{\mathrm{HS}}[\rho(\mathbf{r})]$ is the free energy per particle of the hard-sphere fluid (accurately described by the Carnahan-Starling equation of state), including the ideal gas contribution. The contribution due to the long-range van der Waals forces is included in the mean-field manner. To be specific, we consider a full Lennard-Jones (LJ) 12-6 potential to model the fluid-fluid attraction according to the Barker-Henderson perturbative scheme

$$\phi(r) = \begin{cases} 0, & r < \sigma \\ 4\varepsilon\left[\left(\frac{\sigma}{r}\right)^{12} - \left(\frac{\sigma}{r}\right)^{6}\right], & r \geqslant \sigma, \end{cases} \tag{2}$$

where for the sake of simplicity the LJ parameter σ is taken equal to the hard-sphere diameter.

The free-energy functional $\mathcal{F}[\rho]$ describes the intrinsic properties of a given fluid. The total free energy, including also a contribution of the external field, is related to the grand potential functional through the Legendre transform

$$\Omega[\rho] = \mathcal{F}[\rho] + \int \rho(\mathbf{r})\,[V(\mathbf{r}) - \mu]\,d\mathbf{r}, \tag{3}$$

where μ is the chemical potential and $V(\mathbf{r})$ is the external field due to the presence of a wall $W \subset \mathbb{R}^3$,

$$V(\mathbf{r}) = \begin{cases} \infty, & \mathbf{r} \in W \\ \rho_w \int_W \phi_w(|\mathbf{r} - \mathbf{r}'|)\,d\mathbf{r}' & \text{elsewhere,} \end{cases} \tag{4}$$

consisting of the atoms interacting with the fluid particles via the LJ potential $\phi_w(r)$, with the parameters σ_w and ε_w, and uniformly distributed throughout the wall with a density ρ_w:

$$\phi_w(r) = 4\varepsilon_w\left[\left(\frac{\sigma_w}{r}\right)^{12} - \left(\frac{\sigma_w}{r}\right)^{6}\right]. \tag{5}$$

Applying the variational principle to the grand potential functional, Eq. (3), we attain the Euler-Lagrange equation:

$$\frac{\delta\mathcal{F}_{\mathrm{HS}}[\rho]}{\delta\rho(\mathbf{r})} + \int \rho(\mathbf{r}')\phi(|\mathbf{r} - \mathbf{r}'|)\,d\mathbf{r}' + V(\mathbf{r}) - \mu = 0, \tag{6}$$

where $\mathcal{F}_{\mathrm{HS}}[\rho]$ denotes the first term in the right-hand side of Eq. (1). In general, the solution to Eq. (6) comprises all extremes of the grand potential $\Omega[\rho]$ as given by Eq. (3) and not just the global minimum corresponding to the equilibrium state. Here we develop a pseudo arc-length continuation scheme for the numerical computation of Eq. (6) that enables us to capture both locally stable and unstable solutions and thus to construct the entire bifurcation diagrams for the isotherms (details of the scheme are given in Appendix A).

The excess part of the grand potential functional (3) over the bulk may be expressed in the form

$$\begin{aligned}\Omega_{\mathrm{ex}}[\rho(\mathbf{r})] = &-\int \{p[\rho(\mathbf{r})] - p(\rho_b)\}\,d\mathbf{r} \\ &+ \frac{1}{2}\iint \rho(\mathbf{r})[\rho(\mathbf{r}') - \rho(\mathbf{r})]\phi(|\mathbf{r}' - \mathbf{r}|)d\mathbf{r}'\,d\mathbf{r} \\ &+ \int \rho(\mathbf{r})V(\mathbf{r})\,d\mathbf{r},\end{aligned} \tag{7}$$

where ρ_b is the density of the bulk phase and

$$-p(\rho) = \rho f_{\mathrm{HS}}(\rho) + \alpha\rho^2 - \mu\rho \tag{8}$$

is the negative pressure, or grand potential per unit volume, of a system with uniform density ρ and $\alpha \equiv \frac{1}{2}\int \phi(|\mathbf{r}|)d\mathbf{r} = -\frac{16}{9}\pi\varepsilon\sigma^3$. In particular, the equilibrium value of the excess grand potential (7) per unit area of a two-phase system of liquid and vapor in the absence of an external field, yields the surface tension between the coexisting phases, γ_{lg}. The prediction of γ_{lg} as given by the minimization of Eq. (7) agrees fairly well with both computations and experimental data, as shown in Fig. 1.

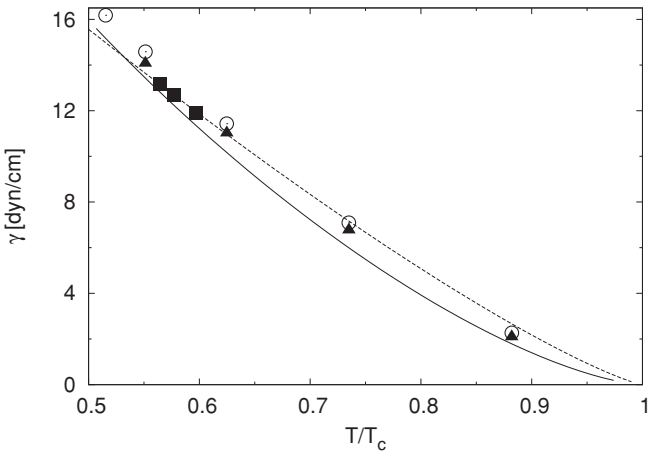

FIG. 1. Plots of surface tension as a function of dimensionless temperature, T/T_c. Solid line: numerical DFT results of our model scaled with $\varepsilon/k_B = 119.8$ K and $\sigma = 3.4$ Å; triangles: computational results by Toxvaerd for a 12-6 LJ fluid using the Barker-Henderson perturbation theory [13] with the Percus-Yevick solution [14] for the hard-sphere reference fluid and using the exact hard-sphere diameter [15]; circles: Monte Carlo simulations by Lee and Barker [16]; squares: experimental results for argon by Guggenheim [17]; dashed line: fit of experimental results to equation $\gamma(T) = \gamma_0(1 - T/T_c)^{1+r}$ by Guggenheim [17]. The resulting coefficients are $\gamma_0 = 36.31$ dyn/cm and $r = \frac{2}{9}$.

B. Translational symmetry: Planar wall

If the general formalism outlined above is applied on a particular external field attaining a certain symmetry, it will adopt a significantly simpler form. In the next section we will formulate the basic equations resulting from the equilibrium conditions obtained from the minimization of Eq. (7), for a spherical model of the external field, i.e., a system with rotational symmetry. But prior to that, it is instructive to discuss the zero-curvature limit of the above model, corresponding to an adsorbed LJ fluid on a planar wall, a system with translational symmetry.

For a planar substrate $W = \mathbb{R}^2 \times \mathbb{R}^-$ in Cartesian coordinates, the density profile is only a function of z, so that the Euler-Lagrange equation reads

$$\begin{aligned}&\mu_{\mathrm{HS}}[\rho(z)] + \int_0^\infty \rho(z')\Phi_{\mathrm{Pla}}(|z - z'|)\,dz' \\ &\quad + V_\infty(z) - \mu = 0 \quad (\forall z \in \mathbb{R}^+),\end{aligned} \tag{9}$$

where $\mu_{\mathrm{HS}}[\rho] = \frac{\partial[f_{\mathrm{HS}}(\rho)\rho]}{\partial\rho}$ is the chemical potential of the hard-sphere system. A fluid particle at a distance z from the wall experiences the wall potential:

$$\begin{aligned}V_\infty(z) &= \rho_w \int_W \phi_w\left(\sqrt{x'^2 + y'^2 + (z - z')^2}\right)dx'\,dy'\,dz' \\ &= \begin{cases} \infty, & z \leqslant 0 \\ 4\pi\rho_w\varepsilon_w\sigma_w^3\left[\frac{1}{45}\left(\frac{\sigma_w}{z}\right)^9 - \frac{1}{6}\left(\frac{\sigma_w}{z}\right)^3\right], & z > 0. \end{cases}\end{aligned} \tag{10}$$

$\Phi_{\mathrm{Pla}}(z)$ in Eq. (9) is the surface potential exerted by the fluid particles uniformly distributed (with a unit density) over the

x-y plane at distance z:

$$\Phi_{\rm Pla}(z) = \iint \phi(\sqrt{x^2+y^2+z^2})\,dy\,dx$$
$$= 2\pi \int_0^\infty \phi(\sqrt{z^2+r^2})\,r\,dr$$
$$= -\frac{6}{5}\pi\varepsilon\sigma^2 \times \begin{cases} 1, & z < \sigma \\ \frac{5}{3}\left(\frac{\sigma}{z}\right)^4 - \frac{2}{3}\left(\frac{\sigma}{z}\right)^{10}, & z \geqslant \sigma. \end{cases} \quad (11)$$

In the framework of DFT, the natural order parameter for wetting transitions is the Gibbs adsorption per unit area:

$$\Gamma_\infty[\rho(z)] = \int_0^\infty [\rho(z) - \rho_b]\,dz. \quad (12)$$

C. Rotational symmetry: Spherical wall

If the external field is induced by a spherical wall, $W = \{\mathbf{r} \in \mathbb{R}^3 : r \equiv |\mathbf{r}| < R\}$, the variational principle yields

$$\mu_{\rm HS}[\rho(r)] + \int_R^\infty \rho(r')\Phi_{\rm Sph}(r,r')dr' + V_R(r) - \mu = 0 \qquad (\forall r > R), \quad (13)$$

where $\Phi_{\rm Sph}(r,r')$ is the surface interaction potential per unit density generated by fluid particles uniformly distributed on the surface of the sphere $B_{r'}$ centered at the origin at distance r,

$$\Phi_{\rm Sph}(r,r') = \int_{\partial B_{r'}} \phi(|\mathbf{r}-\tilde{\mathbf{r}}|)\,d\tilde{\mathbf{r}}$$
$$= \frac{r'}{r}[\Phi_{\rm Pla}(|r-r'|) - \Phi_{\rm Pla}(|r+r'|)] \quad (14)$$

(see also Appendix B 1). The wall potential in Eq. (4) for the spherical wall, $W = \{\mathbf{r} \in \mathbb{R}^3 : r \equiv |\mathbf{r}| < R\}$, is

$$V_R(r) = \frac{\rho_w\varepsilon_w\sigma_w^4\pi}{3r}\left\{\frac{\sigma_w^8}{30}\left[\frac{r+9R}{(r+R)^9} - \frac{r-9R}{(r-R)^9}\right] + \sigma_w^2\left[\frac{r-3R}{(r-R)^3} - \frac{r+3R}{(r+R)^3}\right]\right\}. \quad (15)$$

Replacing the distance from the origin r by the radial distance from the wall $\tilde{r} = r - R$, one can easily see that the external potential (15) reduces to the planar wall potential (10), for $R \to \infty$. Analogously to the planar case, we define the adsorption Γ_R as the excess number of particles of the system with respect to the surface of the wall:

$$\Gamma_R[\rho(r)] = \int_R^\infty \left(\frac{r}{R}\right)^2 [\rho(r) - \rho_b]\,dr. \quad (16)$$

III. WETTING ON A PLANAR SUBSTRATE

In this section we make a comparison between the numerical solution of DFT and the prediction given by the effective interfacial Hamiltonian according to SKA for the first-order wetting transition on a planar substrate. More specifically, we consider a planar semi-infinite wall interacting with the fluid according to Eq. (10) with the typical parameters $\rho_w\varepsilon_w = 0.8\varepsilon/\sigma^3$ and $\sigma_w = 1.25\sigma$ that correspond to the class of intermediate-substrate systems [18] for which prewetting phase transitions can be observed. We note that wetting on planar and spherical walls is a multiparametric problem, and hence a full parametric study of the global phase diagram is a difficult task, beyond the scope of this paper.

A. Numerical DFT results of wetting on a planar wall

Figure 2 depicts the surface-phase diagram of the considered model in the $(\Delta\mu, T)$ plane, where $\Delta\mu = \mu - \mu_{\rm sat}$ is the departure of the chemical potential from its saturation value. The first-order wetting transition takes place at wetting temperature $k_BT_w = 0.621\varepsilon$, well below the critical temperature of the bulk fluid $k_BT_c = 1.006\varepsilon$ for our model. The prewetting line connects the saturation line at the wetting temperature T_w and terminates at the prewetting critical point, $k_BT_{\rm pwc} = 0.724\varepsilon$. The slope of the prewetting line is governed by a

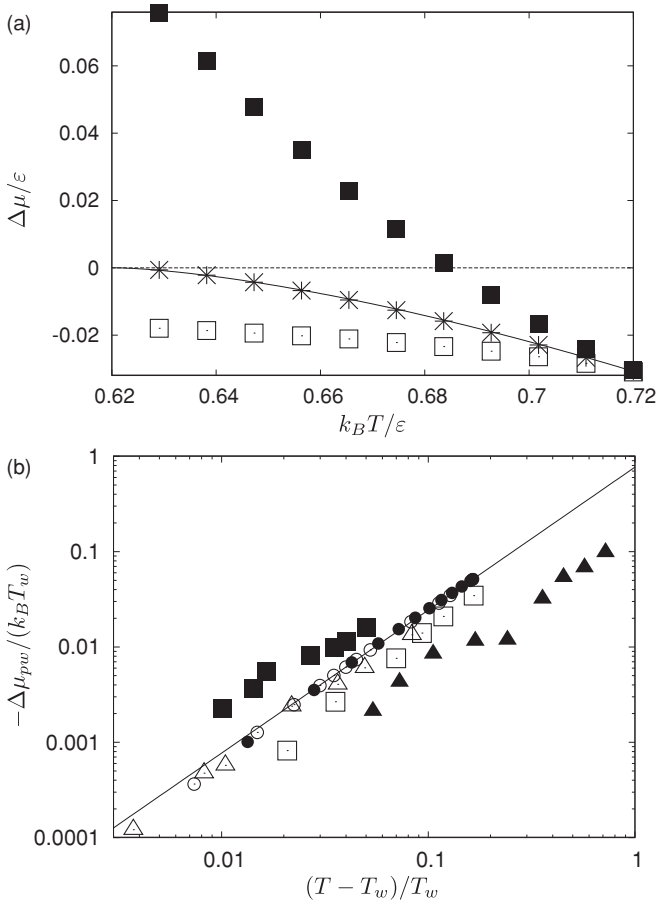

FIG. 2. (a) Deviation of the chemical potential from its saturation value at prewetting (crosses), and at the left (open squares) and right (filled squares) saddle nodes of bifurcation as a function of temperature. The dashed line marks the locus of the chemical potential at saturation for the given temperature, $\Delta\mu = 0$. The solid line is a fit to $-\Delta\mu_{\rm pw}(T)/(k_BT_w) = C[(T-T_w)/T_w]^{3/2}$, where the wetting temperature is $k_BT_w = 0.621\varepsilon$ and the prewetting critical temperature is $k_BT_{\rm pwc} = 0.724\varepsilon$. The resulting coefficient is $C = 0.77$. (b) Scaled prewetting phase diagrams for different systems. The circles are DFT calculations for an attractive wall with $\sigma_w = 1.25\sigma$ and $\rho_w\varepsilon_w = 0.8\varepsilon/\sigma^3$ (open circles) and $\rho_w\varepsilon_w = 0.75\varepsilon/\sigma^3$ (filled circles). Experimental data [21]: filled squares, methanol on cyclohexane [22]; open triangles, H_2 on rubidium [23]; filled triangles, He on caesium [24]; and open squares, H_2 on caesium [25].

Clapeyron-type equation [19], which, in particular, states that the prewetting line approaches the saturation line tangentially at T_w with

$$\left.\frac{d(\Delta\mu_{\rm pw})}{dT}\right|_{T=T_w} = 0, \tag{17}$$

in line with our numerical computations. Schick and Taborek [20] later showed that the prewetting line scales as $-\Delta\mu \sim (T - T_w)^{3/2}$. In Ref. [21], this power law was confirmed experimentally, such that

$$-\frac{\Delta\mu_{\rm pw}(T)}{k_B T_w} = C\left(\frac{T - T_w}{T_w}\right)^{3/2}, \tag{18}$$

with $C \approx \frac{1}{2}$. A fit of our DFT results with Eq. (18) leads to a coefficient $C = 0.77$, in reasonable agreement with the experimental data (see Fig. 2).

Figure 3 depicts the adsorption isotherm in terms of the thickness of the adsorbed liquid film ℓ as a function of $\Delta\mu$ for the temperature $k_B T = 0.7\varepsilon$ in the interval between the wetting temperature T_w and the prewetting critical temperature $T_{\rm pwc}$. ℓ can be associated with the Gibbs adsorption through

$$\ell = \frac{\Gamma_R[\rho]}{\Delta\rho}, \tag{19}$$

for both finite and infinite R, where $\Delta\rho = \rho_l^{\rm sat} - \rho_g^{\rm sat}$ is the difference between the liquid and gas densities at saturation.

The isotherm exhibits a van der Waals loop with two turning points depicted as B and C demarcating the unstable branch. Points A and D indicate the equilibrium between thin and thick layers, corresponding to a point on the prewetting line in Fig. 2. The location of the equilibrium points can be obtained from a Maxwell construction. Details of the numerical scheme we developed for tracing the adsorption isotherms are given in Appendix A.

B. SKA for a planar wall

For the sake of clarity and completeness we briefly review the main features of SKA for a planar geometry (details are given in Ref. [1]).

Let us consider a liquid film of thickness ℓ adsorbed on a planar wall. According to SKA the density distribution is approximated by a piecewise constant function

$$\rho_\ell^{\rm SKA}(z) = \begin{cases} 0, & z < \delta \\ \rho_l^+, & \delta < z < \ell \\ \rho_g, & z > \ell\,, \end{cases} \tag{20}$$

where ρ_g is the density of the gas reservoir and ρ_l^+ is the density of the metastable liquid at the same thermodynamic conditions stabilized by the presence of the planar wall, Eq. (10) and $\delta \approx \frac{1}{2}(\sigma + \sigma_w)$. The off coexistence of the two phases induces the pressure difference

$$p^+(\mu) - p(\mu) \approx \Delta\rho\Delta\mu, \tag{21}$$

where p^+ is the pressure of the metastable liquid and p is the pressure of the gas reservoir, and where we assume that $\Delta\mu = \mu - \mu_{\rm sat} < 0$ is small.

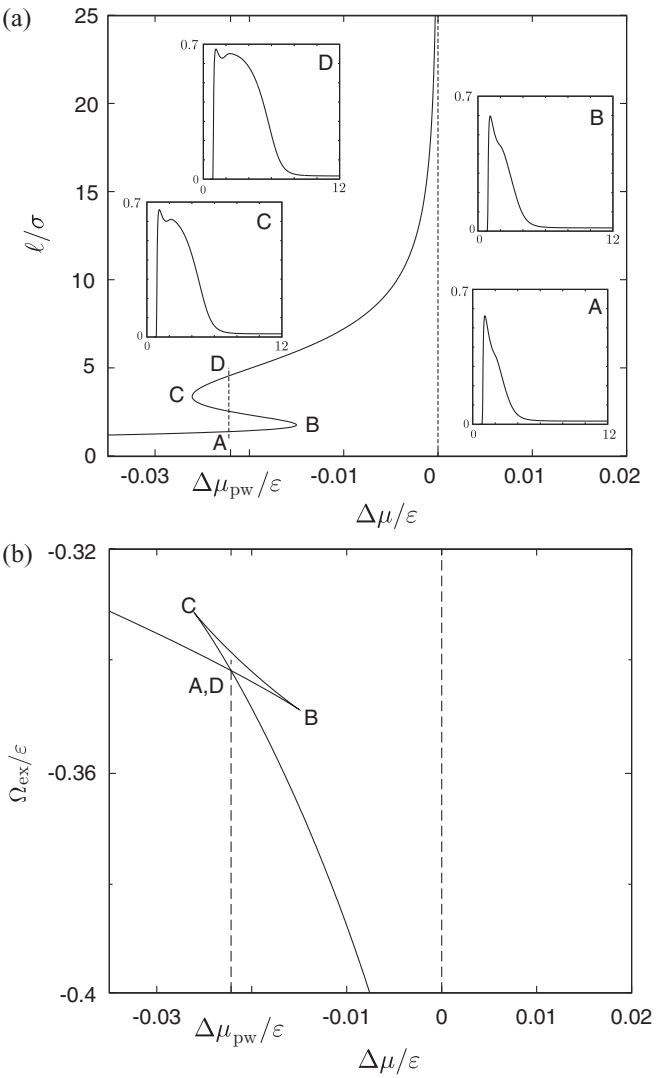

FIG. 3. (a) ℓ-$\Delta\mu$ bifurcation diagram for $k_B T = 0.7\varepsilon$ for a wall with $\rho_w\varepsilon_w = 0.8\varepsilon/\sigma^3$ and $\sigma_w = 1.25\sigma$. $\Delta\mu$ is the deviation of the chemical potential from its saturation value, $\mu_{\rm sat}$. The prewetting transition, marked by the dashed line, occurs at chemical potential $\Delta\mu_{\rm pw} = -0.022\varepsilon$. The inset subplots show the density $\rho\sigma^3$ as a function of the distance z/σ from the wall. (b) Excess grand potential $\Omega_{\rm ex}/\varepsilon$ as a function of $\Delta\mu/\varepsilon$ in the vicinity of the prewetting transition.

The excess grand potential per unit area $\mathcal{A}$ of the system then can be expressed in terms of macroscopic quantities as a function of ℓ

$$\frac{\Omega_{\rm ex}(\ell;\mu)}{\mathcal{A}} = -\Delta\mu\Delta\rho(\ell - \delta) + \gamma_{wl}^{\rm SKA}(\mu) + \gamma_{lg}^{\rm SKA} + w^{\rm SKA}(\ell;\mu), \tag{22}$$

where $\gamma_{wl}^{\rm SKA}$ and $\gamma_{lg}^{\rm SKA}$ are the SKAs to the wall-liquid and the liquid-gas surface tensions, respectively, and $w^{\rm SKA}(\ell)$ is the effective potential between the two interfaces (binding potential). In the following, we will suppress the explicit μ dependence of these quantities.

The link with the microscopic theory can be made if the contributions in the right-hand side of Eq. (22) are expressed in terms of our molecular model, which, when summed up,

give the excess grand potential (7), where we have substituted the ansatz (20):

$$\begin{aligned}\gamma_{wl}^{\mathrm{SKA}} &= -\frac{\rho_l^{+2}}{2}\int_{-\infty}^{0}\int_{0}^{\infty}\Phi_{\mathrm{Pla}}(|z-z'|)\,dz'\,dz \\ &\quad + \rho_l^{+}\int_{\delta}^{\infty}V_{\infty}(z)\,dz \\ &= \frac{3}{4}\pi\varepsilon\sigma^4\rho_l^{+2} + \frac{\pi}{90\delta^8}\left(\sigma_w^6 - 30\delta^6\right)\sigma_w^6\rho_w\varepsilon_w\rho_l^{+},\end{aligned} \tag{23}$$

$$\begin{aligned}\gamma_{lg}^{\mathrm{SKA}} &= -\frac{\Delta\rho^2}{2}\int_{-\infty}^{0}\int_{0}^{\infty}\Phi_{\mathrm{Pla}}(|z-z'|)\,dz'\,dz \\ &= \frac{3}{4}\pi\varepsilon\sigma^4\Delta\rho^2,\end{aligned} \tag{24}$$

$$\begin{aligned}w^{\mathrm{SKA}}(\ell) &= \Delta\rho\left(\rho_l^{+}\int_{\ell-\delta}^{\infty}\int_{z}^{\infty}\Phi_{\mathrm{Pla}}(z')\,dz'\,dz\right. \\ &\quad \left. - \int_{\ell}^{\infty}V_{\infty}(z)\,dz\right) \\ &= -\frac{A}{12\pi\ell^2}\left(1 + \frac{2+3\frac{\delta}{\ell}}{1-\frac{\rho_w\varepsilon_w\sigma_w^6}{\rho_l^{+}\varepsilon\sigma^6}}\frac{\delta}{\ell} + O\left((\delta/\ell)^3\right)\right),\end{aligned} \tag{25}$$

where we considered the distinguished limit $\delta \ll \ell$. A is the Hamaker constant given by:

$$A = 4\pi^2\Delta\rho\left(\rho_l^{+}\varepsilon\sigma^6 - \rho_w\varepsilon_w\sigma_w^6\right). \tag{26}$$

We note that the Hamaker constant is implicitly temperature dependent and that the attractive contribution of the potential of the wall enables the Hamaker constant to change its sign. Hence, in contrast with adsorption on a hard wall, where the Hamaker constant is always negative, there may be a temperature below which its sign is positive (large ρ_l) and negative above. Clearly, complete wetting is only possible for $A < 0$.

Making use of only the leading-order term in Eq. (25), the minimization of Eq. (22) with respect to ℓ gives

$$\Delta\rho\Delta\mu - \frac{A}{6\pi\ell^3} \approx 0. \tag{27}$$

Hence, at this level of approximation the equilibrium thickness of the liquid film is

$$\ell_{\mathrm{eq}} \approx \left(\frac{A}{6\pi\Delta\rho\Delta\mu}\right)^{1/3}. \tag{28}$$

When substituted into Eq. (22), the wall-gas surface tension to leading order reads

$$\gamma_{wg}^{\mathrm{SKA}} = \gamma_{wl}^{\mathrm{SKA}} + \gamma_{lg}^{\mathrm{SKA}} + \left(-\frac{9A}{16\pi}\right)^{1/3}|\Delta\rho\Delta\mu|^{2/3}. \tag{29}$$

Equation (28) can be confirmed by a comparison against numerical DFT (see Fig. 4). We observe that the prediction of SKA becomes reliable for $|\Delta\mu| < 0.01\varepsilon$, corresponding to a somewhat surprisingly small value of the liquid film, $\ell \approx 5\sigma$. Beyond this value, the coarse-grained approach loses its validity, and also, the prewetting transition is approached, both of which cause the curve in Fig. 4 to bend (see also Fig. 3).

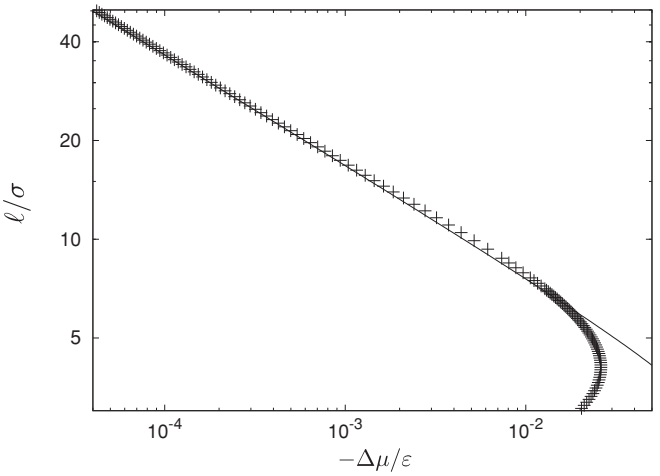

FIG. 4. Ln-ln plot of the film thickness as a function of deviation of the chemical potential from saturation, $\Delta\mu$, for $k_BT = 0.7\varepsilon$ and wall parameters $\rho_w\varepsilon_w = 0.8\varepsilon/\sigma^3$ and $\sigma_w = 1.25\sigma$. The crosses are results from DFT computations. The solid line is the analytical prediction in Eq. (27) obtained from SKA.

It is worth noting that the only term in Eq. (22) having an ℓ dependence and thus governing the wetting behavior, is the term related to the undersaturation pressure and the binding potential, $w^{\mathrm{SKA}}(\ell)$. Clearly, γ_{lg} does not come into play in the planar case since the translation of the liquid-gas interface along the z axis does not change the free energy of the system. The situation becomes qualitatively different if the substrate is curved. Nevertheless, at this stage we conclude in line with earlier studies, that SKA provides a fully satisfactory approach to the first-order wetting transition on a planar wall.

IV. WETTING ON A CURVED SUBSTRATE

A. SKA for the spherical wall

For the spherical geometry, SKA adopts the following form:

$$\rho_{R,\ell}^{\mathrm{SKA}}(r) = \begin{cases} 0, & r < R+\delta \\ \rho_l^{+}, & R+\delta < r < R+\ell \\ \rho_g, & R+\ell < r < \infty. \end{cases} \tag{30}$$

The corresponding excess grand potential now reads

$$\begin{aligned}\frac{\Omega_{\mathrm{ex}}(\mu,R,\ell)}{4\pi R^2} &= -\Delta\mu\Delta\rho\frac{(R+\ell)^3-\tilde{R}^3}{3R^2} + \gamma_{wl}^{\mathrm{SKA}}(R) \\ &\quad + \gamma_{lg}^{\mathrm{SKA}}(R+\ell)\left(1+\frac{\ell}{R}\right)^2 + w^{\mathrm{SKA}}(\ell;R),\end{aligned} \tag{31}$$

where $\tilde{R} = R + \delta$. Within this approximation, the liquid-vapor surface tension becomes (see also Appendix B)

$$\gamma_{lg}^{\mathrm{SKA}}(R) = \gamma_{lg}^{\mathrm{SKA}}(\infty)\left\{1 - \frac{2}{9}\frac{\ln(R/\sigma)}{(R/\sigma)^2} + O\left((\sigma/R)^2\right)\right\} \tag{32}$$

and an analogous expansion holds for $\gamma_{wl}^{\mathrm{SKA}}(R)$. The $\frac{\ln(R/\sigma)}{(R/\sigma)^2}$ correction to $\gamma_{lg}^{\mathrm{SKA}}(\infty)$ is due to the r^{-6} decay of our model. We note that short-range potentials lead to different curvature dependence of the surface tension, a point that has been

discussed in detail in Refs. [7,8,26]. Interestingly, the $O(\sigma/R)$ correction to the surface tension, as one would expect from the Tolman theory [27], is missing. It corresponds to a vanishing Tolman length within SKA, as we will explicitly show in the following section. Although the value of the Tolman length is still a subject of some controversy, it is most likely that its value is nonzero, unless the system is symmetric under interchange between the two coexisting phases [28]. This observation has been confirmed numerically in Ref. [8] from a fit of DFT results for the wall-gas surface tension in a nondrying regime for the hard-wall substrate. Thus, the linear term was included by hand into the expansion (32) [8].

Finally, the binding potential within SKA for the spherical wall yields

$$w^{\mathrm{SKA}}(\ell;R) = w^{\mathrm{SKA}}(\ell;\infty)\left(1+\frac{\ell}{R}\right), \tag{33}$$

where terms $O\left((\delta/\ell)^3, \delta/R, \frac{\ln(\ell/R)}{(R/\ell)^2}\right)$ have been neglected.

B. SIA for the spherical wall

As an alternative to SKA, Napiórkowski and Dietrich [10] proposed a modified version of the effective Hamiltonian, in which the liquid-gas interface was approximated in a less crude way by a continuous monotonic function, the SIA. Applied for the second-order wetting transition on a planar wall, SIA merely confirmed that SKA provides a reliable prediction for such a system. Formulated now for the spherical case, the density profile of the fluid takes the form

$$\rho^{\mathrm{SIA}}_{R,\ell}(r) = \begin{cases} 0, & r < R+\delta \\ \rho_l^+, & R+\delta < r < R+\ell-\frac{\chi}{2} \\ \rho_{lg}(r-R-\ell), & R+\ell-\frac{\chi}{2} < r < R+\ell+\frac{\chi}{2} \\ \rho_g & R+\ell+\frac{\chi}{2} < r < \infty. \end{cases} \tag{34}$$

Thus, a nonzero width of the liquid-vapor interface, χ, is introduced as an additional parameter. The density profile $\rho_{lg}(\cdot)$ in this region is not specified, but the following constraints are imposed:

$$\rho_{lg}\left(-\frac{\chi}{2}\right) = \rho_l^+ \quad \text{and} \quad \rho_{lg}\left(\frac{\chi}{2}\right) = \rho_g, \tag{35}$$

with an additional assumption of a monotonic behavior of the function $\rho_{lg}(r)$. An illustrative example of $\rho^{\mathrm{SIA}}_{R,\ell}(r)$ is given in Fig. 5. The corresponding excess grand potential takes the form

$$\frac{\Omega_{\mathrm{ex}}}{4\pi R^2} = -\Delta\mu\Delta\rho\frac{(R+\ell)^3-\tilde{R}^3}{3R^2} + \gamma_{wl}^{\mathrm{SIA}}(R) + \left(1+\frac{\ell}{R}\right)^2\gamma_{lg}^{\mathrm{SIA}}(R+\ell) + w^{\mathrm{SIA}}(R,\ell), \tag{36}$$

taking $R+\ell$ as the Gibbs dividing surface (so that ℓ is a measure of the number of particles adsorbed at the wall).

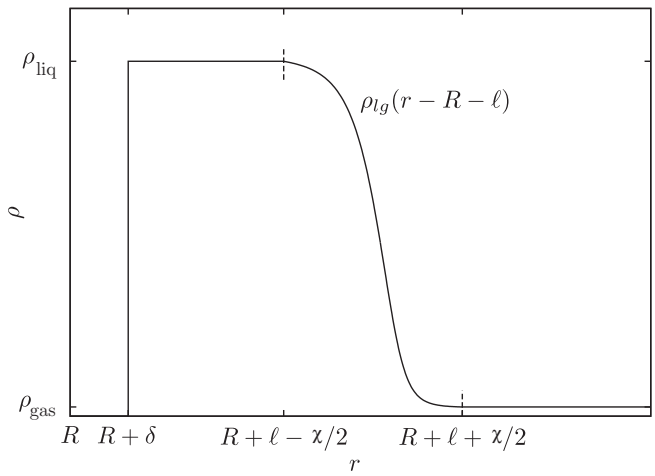

FIG. 5. Sketch of the density profile according to SIA for a certain film thickness ℓ. A piecewise function approximation is employed so that except for the interval $(R+\ell-\chi/2, R+\ell+\chi/2)$ the density is assumed to be piecewise constant.

The binding potential (see also Appendix C 3) is obtained from

$$w^{\mathrm{SIA}}(R,\ell) = \rho_l^+\int_{R+\ell-\chi/2}^{\infty}\left[\rho_l^+ - \rho^{\mathrm{SIA}}_{R,\ell}(r)\right]\Psi_{R+\delta}(r)\left(\frac{r}{R}\right)^2 dr - \int_{R+\ell-\chi/2}^{\infty}\left[\rho_l^+ - \rho^{\mathrm{SIA}}_{R,\ell}(r)\right]V_R(r)\left(\frac{r}{R}\right)^2 dr, \tag{37}$$

where $\Psi_R(r) = \int_0^R \Phi_{\mathrm{Sph}}(r,r')dr'$—see Appendix B 1 for the explicit form of the last expression.

The wall-liquid surface tension remains unchanged compared to that obtained from SKA, Eq. (24). However, the liquid-gas surface tension now reads (see Appendix C 1)

$$\gamma_{lg}^{\mathrm{SIA}}(R) = -\int_{R-\chi/2}^{R+\chi/2}\{p[\rho_{lg,R}(r)] - p_{\mathrm{ref}}\}\left(\frac{r}{R}\right)^2 dr + \frac{1}{2}\int_0^{\infty}\int_0^{\infty}\rho_{lg,R}(r)[\rho_{lg,R}(r') - \rho_{lg,R}(r)] \times \Phi_{\mathrm{Sph}}(r,r')\left(\frac{r}{R}\right)^2 dr'\,dr, \tag{38}$$

where p_{ref} is the pressure at saturation.

From now on, we neglect the curvature dependence of χ and $\rho_{lg,R}(\cdot)$, as they would introduce higher-order corrections not affecting the asymptotic results at our level of approximation. This is also in line with previous studies which show that the Tolman length only depends on the density profile in the planar limit [28]. Then Eq. (38) can be written as

$$\gamma_{lg}^{\mathrm{SIA}}(R) = \gamma_{lg}^{\mathrm{SIA}}(\infty)\left[1 - \frac{2\delta_\infty}{R} + O\left(\frac{\ln(R/\sigma)}{(R/\sigma)^2}\right)\right], \tag{39}$$

where δ_∞ is the Tolman length of the liquid-gas surface tension, as given by (Appendix C 2)

$$\delta_\infty = \frac{1}{\gamma_{lg}^{\mathrm{SIA}}(\infty)}\int_{-\chi/2}^{\chi/2}\{p[\rho_{lg}(z)] - p_{\mathrm{ref}}\}z\,dz. \tag{40}$$

The Tolman length is independent of the choice of the dividing surface. We also note that an immediate consequence of Eq. (40) is that within SKA the Tolman length vanishes.

The equilibrium film thickness then follows from setting the derivative of Eq. (36) with respect to ℓ equal to zero:

$$\begin{aligned}\frac{1}{4\pi R^2}\frac{d\Omega_{\rm ex}}{d\ell} &= -\Delta\mu\Delta\rho\left(1+\frac{\ell}{R}\right)^2+\frac{2}{R}\left(1+\frac{\ell}{R}\right)\\ &\times\gamma_{lg}^{\rm SIA}(R+\ell)+\left(1+\frac{\ell}{R}\right)^2\left.\frac{d\gamma_{lg}^{\rm SIA}}{d\ell}\right|_{R+\ell}\\ &+\rho_l^+\int_{R+\ell-\chi/2}^{R+\ell+\chi/2}\rho_{lg}'(r-R-\ell)\Psi_{R+\delta}(r)\\ &\times\left(\frac{r}{R}\right)^2 dr-\int_{R+\ell-\chi/2}^{R+\ell+\chi/2}\rho_{lg}'(r-R-\ell)\\ &\times V_R(r)\left(\frac{r}{R}\right)^2 dr. \end{aligned}\tag{41}$$

The last two terms of Eq. (41) are of the form

$$\int_{-\chi/2}^{\chi/2}\rho_{lg}'(r)f_{\rm I,II}(R+\ell+r)\,dr,\tag{42}$$

with $f_{\rm I}(r)=\rho_l^+\Psi_{R+\delta}(r)(\frac{r}{R})^2$ and $f_{\rm II}(r)=V_R(r)(\frac{r}{R})^2$. Since $\rho_{lg}(r)$ is monotonic, i.e., ρ_{lg}' does not change sign, the mean value theorem can be employed such that

$$\begin{aligned}&\int_{-\chi/2}^{\chi/2}\rho_{lg}'(r)f_{\rm I,II}(R+\ell+r)\,dr\\ &\quad=-\Delta\rho f_{\rm I,II}(R+\ell+\xi_{\rm I,II}),\end{aligned}\tag{43}$$

for some $\xi_{\rm I,II}\in(-\chi/2,\chi/2)$, where we made use of $\int\rho_{lg}'(r)dr=-\Delta\rho$. Substituting Eq. (43) into Eq. (41) and setting the resulting expression equal to zero, we obtain

$$\begin{aligned}\Delta\mu &= \frac{1}{\Delta\rho}\left(\frac{2\gamma_{lg}^{\rm SIA}(R+\ell)}{R+\ell}+\left.\frac{d\gamma_{lg}^{\rm SIA}}{d\ell}\right|_{R+\ell}\right)\\ &-\rho_l^+\Psi_{R+\delta}(R+\ell+\xi_{\rm I})\left(1+\frac{\xi_{\rm I}}{R+\ell}\right)^2\\ &+V_R(R+\ell+\xi_{\rm II})\left(1+\frac{\xi_{\rm II}}{R+\ell}\right)^2.\end{aligned}\tag{44}$$

So far, there is no approximation within SIA. Equation (44) can be simplified by appropriately estimating the values of the auxiliary parameters $\xi_{\rm I}$ and $\xi_{\rm II}$. To this end, we employ a simple linear approximation to the density profile at the liquid-gas interface, taking $-\rho_{lg}'(r)/\Delta\rho\approx 1/\chi$ in Eq. (43). Furthermore, we expand $f_{\rm I,II}$ in powers of $\ell/R,\sigma/\ell$,

$$\begin{aligned}f_{\rm I}(R+\ell+r) &= -\frac{2\pi\rho_l^+\varepsilon\sigma^6}{3(\ell+r-\delta)^3}\left[1+\frac{\ell+r+3\delta}{2R}\right.\\ &\left.+O\left(\left(\frac{\sigma}{\ell}\right)^6,\left(\frac{\ell}{R}\right)^2\right)\right],\end{aligned}\tag{45}$$

$$\begin{aligned}f_{\rm II}(R+\ell+r) &= -\frac{2\pi\rho_w\varepsilon_w\sigma_w^6}{3(\ell+r)^3}\left[1+\frac{\ell+r}{2R}\right.\\ &\left.+O\left(\left(\frac{\sigma}{\ell}\right)^6,\left(\frac{\ell}{R}\right)^2\right)\right],\end{aligned}\tag{46}$$

where we assumed the distinguished limits $r,\delta,\sigma\ll\ell\ll R$. Inserting Eqs. (45) and (46) into Eq. (43) yields for $\xi_{\rm I,II}$:

$$\xi_{\rm I,II}=-\frac{\chi^2}{6\ell}\left[1+O\left(\frac{\delta}{\ell},\frac{\ell}{R},\left(\frac{\chi}{\ell}\right)^2\right)\right].\tag{47}$$

From Eq. (44), we obtain to leading order,

$$\begin{aligned}&\rho_l^+\Psi_{R+\delta}(R+\ell+\xi_{\rm I})\left(1+\frac{\xi_{\rm I}}{R+\ell}\right)^2\\ &\quad=-\frac{2\pi}{3\ell^3}\rho_l^+\varepsilon\sigma^6\left[1+O\left(\frac{\delta}{\ell},\frac{\ell}{R},\left(\frac{\chi}{\ell}\right)^2\right)\right],\end{aligned}\tag{48}$$

$$\begin{aligned}&V_R(R+\ell+\xi_{\rm II})\left(1+\frac{\xi_{\rm II}}{R+\ell}\right)^2\\ &\quad=-\frac{2\pi}{3\ell^3}\rho_w\varepsilon_w\sigma_w^6\left[1+O\left(\frac{\ell}{R},\left(\frac{\chi}{\ell}\right)^2\right)\right].\end{aligned}\tag{49}$$

Finally, substituting Eqs. (48) and (49) into Eq. (44), we have to leading order

$$\Delta\rho\Delta\mu-\frac{2}{R}\gamma_{lg}^{\rm SIA}(\infty)\approx\frac{A}{6\pi\ell^3},\tag{50}$$

and hence, to leading order the equilibrium wetting film thickness is

$$\ell_{\rm eq}^{\rm SIA}\approx\left(\frac{A}{6\pi\left(\Delta\rho\Delta\mu-2\gamma_{lg,\infty}^{\rm SIA}/R\right)}\right)^{1/3}.\tag{51}$$

We note that this asymptotic analysis can be extended beyond Eq. (51), by including terms $O(\delta/\ell)$, $O(\ell/R)$, and $O((\chi/\ell)^2)$. The latter occurs due to the "soft" treatment of the liquid-vapor interface and is thus not present in SKA.

In Fig. 6 we compare two adsorption isotherms ($k_BT=0.7\varepsilon$) corresponding to wetting on a planar and a spherical wall ($R=100\sigma$). The two curves are mutually horizontally shifted by a practically constant value, in accordance with Eq. (50). This implies that the curve for the spherical wall crosses the saturation line $\Delta\mu=0$ at a finite value of ℓ, and eventually converges to the saturation line as $\Delta\mu^{-1}$ from the right, thus the finite curvature prevents complete wetting. The horizontal shift corresponds to the Laplace pressure contribution, $\Delta\mu=2\gamma_{lg}^{\rm SIA}(\infty)/(\Delta\rho R)$, as verified by comparison with the numerical DFT (Fig. 7). All these conclusions are in line with SKA. However, the difference between SKA and SIA consists in a different treatment of $\gamma_{lg}(\infty)$ [compare Eqs. (B4) and (C2)]. This is quite obvious, since the softness of the interface influences the free energy required to increase the film thickness. We will discuss this point in more detail in the following section.

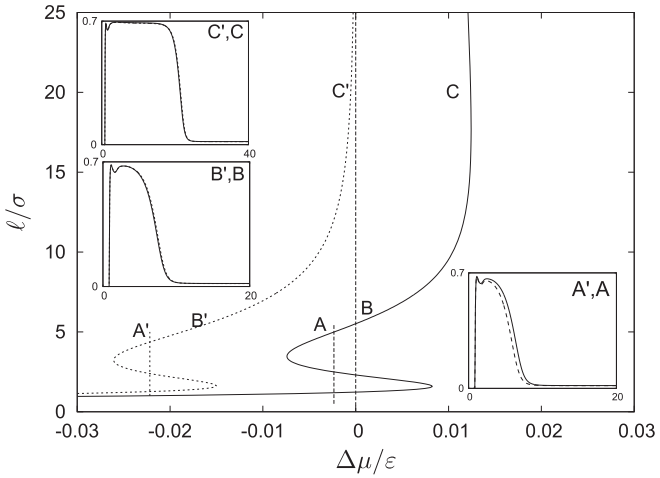

FIG. 6. Isotherms and density profiles for a planar wall (dashed lines) and a sphere with $R = 100\sigma$ (solid lines) at $k_BT = 0.7\varepsilon$ and with wall parameters $\rho_w\varepsilon_w = 0.8\varepsilon/\sigma^3$ and $\sigma_w = 1.25\sigma$. To directly compare the planar to the spherical case, the film thickness instead of adsorption is used as a measure. The subplots in the inset depict the density $\rho\sigma^3$ as a function of the distance from the wall z/σ and $(r - R)/\sigma$ for the planar and the spherical cases, respectively. The points A and A' are at the prewetting transitions. Points B,B' and C,C' correspond to the same film thickness. B is at saturation, whereas C is chosen such that the film thickness ℓ is 20σ.

C. Comparison of SKA and SIA

We now examine the repercussions of the way the liquid-gas interface is treated on the prediction of wetting behavior on a spherical surface. As already mentioned in Sec. IV B, the linear correction in the curvature to the planar liquid-gas surface tension, ignored within SKA, is properly captured by SIA. Furthermore, the presence of the Laplace pressure suggests that the liquid-gas surface tension plays a strong part in the determination of the equilibrium film thickness. This contrasts to the case of a planar geometry, where the term associated with the liquid-gas surface tension has no impact on the equilibrium configuration.

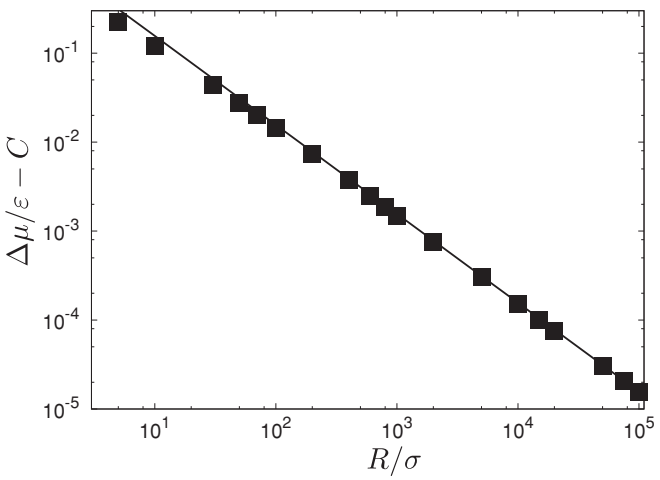

FIG. 7. Numerical verification of Eq. (50). The film thickness ℓ is fixed and corresponds to the adsorption $\Gamma_R = 3.905/\sigma^2$. The solid line corresponds to the analytical result, $\Delta\mu - 2\gamma_{lg}^{\mathrm{SIA}}(\infty)/(\Delta\rho R) = C\varepsilon$, where $\gamma_{lg}^{\mathrm{SIA}}(\infty) = 0.524\varepsilon/\sigma^2$ (see Table I). The symbols denote the numerical DFT results.

TABLE I. Planar surface tensions (Eq. (C2)), Tolman lengths (Eq. (40)), and the corresponding parameters for temperature $k_BT = 0.7\varepsilon$ according to a given auxiliary function approximating the density distribution of the vapor-liquid interface. The parameters are from auxiliary function minimization. The surface tension given by numerical DFT computations is $\gamma_{lg} = 0.517\varepsilon/\sigma^2$ and $\bar{\rho} = (\rho_l + \rho_g)/2$. Note that in the tanh case, the interface width is implicitly determined by the steepness parameter α.

Auxiliary function $\rho_{lg}(z)$	$\gamma_{lg}^{\mathrm{SIA}}(\infty)$	Argument	δ_∞
$\bar{\rho} - \Delta\rho\frac{z}{\chi}$	$0.544\varepsilon/\sigma^2$	$\chi = 4.0\sigma$	-0.07σ
$\bar{\rho} - \frac{3}{2}\Delta\rho\frac{z}{\chi} + 2\Delta\rho(\frac{z}{\chi})^3$	$0.532\varepsilon/\sigma^2$	$\chi = 5.4\sigma$	-0.09σ
$\bar{\rho} - \frac{\Delta\rho}{2}\tanh(\alpha z/\sigma)$	$0.524\varepsilon/\sigma^2$	$\alpha = 0.66$	-0.11σ

To investigate this point in detail, we will first compare the approximations of γ_{lg} as obtained by the two approaches. For this purpose, we start with SIA for a given parametrization of the liquid-gas interface. As shown in Table I, we employ linear, cubic, and hyperbolic tangent auxiliary functions, where the latter violates condition (35) negligibly. The particular parameters are determined by minimization of a given function with respect to the corresponding parameters. In Table I we display the planar liquid-gas surface tension associated with a particular parametrization and the Tolman length resulting from Eq. (40) for the temperature $k_BT = 0.7\varepsilon$. In all three cases the surface tension is close to the one obtained from the numerical solution of DFT and also, the predictions of the Tolman length are in reasonable agreement with the most recent simulation results [29–31], with thermodynamic results [32] as well as with results from the van der Waals square gradient theory [33].

It is reasonable to assume that from the set of considered auxiliary functions, the tanh approximation is the most realistic one, although the numerical results as given in Table I suggest that it is mainly the finite width of the liquid-gas interface, rather than the approximation of the density profile at this region, that matters. To illustrate this, we show in Fig. 8 the dependence of the surface tension on the steepness parameter α, determining the shape of the tanh function. Note that the limit $\alpha \to \infty$ corresponds to the surface tension as predicted by SKA, $\gamma_{lg,\infty}^{\mathrm{SKA}} = 1.060\varepsilon/\sigma^2$, for $k_BT = 0.7\varepsilon$. Such a value contrasts with the result of SIA, which corresponds to the minimum of the function, and yields $\gamma_{lg,\infty}^{\mathrm{SIA}} = 0.524\varepsilon/\sigma^2$, in much better agreement with the numerical solution of DFT, $\gamma_{lg,\infty}^{\mathrm{DFT}} = 0.517\varepsilon/\sigma^2$.

Asymptotic analysis of the film thickness in Eq. (50) reveals that the film thickness for large but finite R remains finite even at saturation with $\ell \sim R^{1/3}$ in line with earlier studies, e.g., Refs. [5,8]. From Eq. (50) one also recognizes a strong dependence of ℓ on the planar liquid-gas surface tension. In Fig. 9 we present the SIA and SKA predictions of the dependence on ℓ as a function of the wall radius. The comparison with the numerical DFT results reveals that for large R, SIA is clearly superior, reflecting a more realistic estimation of the liquid-gas surface tension. For small values of R (and ℓ) we observe a deviation between DFT and the

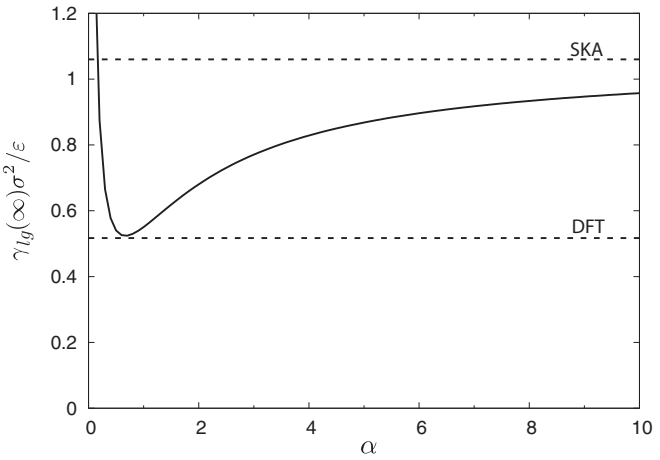

FIG. 8. Plot of a dimensionless planar liquid-gas surface tension for the liquid-gas interface approximation $\rho(z) = \frac{\rho_l+\rho_g}{2} - \frac{\Delta\rho}{2}\tanh(\alpha z/\sigma)$ for $k_BT = 0.7\varepsilon$ as a function of the steepness parameter α. The upper dashed line is the surface tension obtained from SKA, whereas the lower dashed line displays the surface tension obtained from numerical DFT.

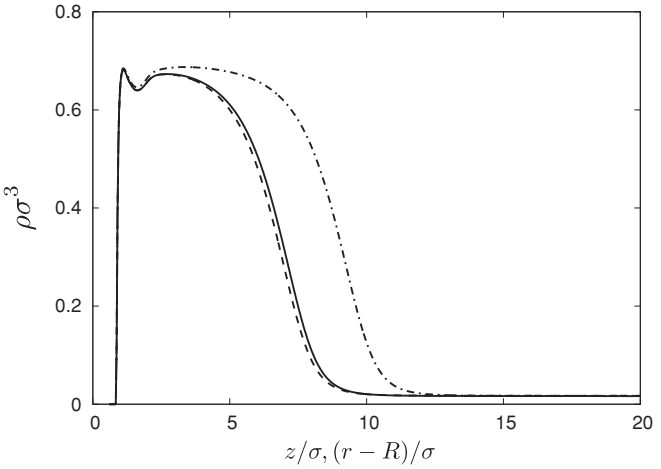

FIG. 10. Density profiles of the fluid adsorbed at the spherical walls of radii $R = 104.1\sigma$ (dashed) and $R = 210.6\sigma$ (dashed-dotted) in a saturated state and at the planar wall (solid line) in an undersaturated state, $\Delta\mu = -0.015\varepsilon$. The wall radii correspond to the equality $2\gamma^j_{lg,\infty}/R = \Delta\rho|\Delta\mu|$ for $j =$ SIA (dashed) and $j =$ SKA (dashed-dotted). $k_BT = 0.7\varepsilon$ and the wall parameters are $\rho_w\varepsilon_w = 0.8\varepsilon/\sigma^3$ and $\sigma_w = 1.25\sigma$.

SIA results. This indicates a limit of validity of our first-order analysis and the assumption of large film thicknesses.

The occurrence of the undersaturation pressure and the Laplace pressure on the left-hand side of Eq. (50) suggests a certain equivalence between the two systems of a planar and a spherical symmetry once the sum of the two pressures is fixed. In Fig. 10 we test this equivalence on the level of a density profile, where DFT results corresponding to the planar and the spherical case are compared, such that $\Delta\rho|\Delta\mu| = 2\gamma^j_{lg}(\infty)/R$, with $j = \{\text{SIA}, \text{SKA}\}$. A high value of $\gamma_{lg}(\infty)$ as given by SKA must now be compensated by a fairly large R. As we have seen in Fig. 6, the high value of R means that the saturation line

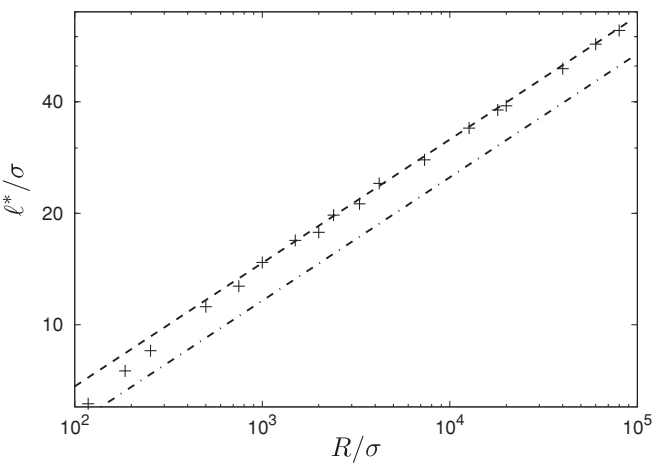

FIG. 9. Film thickness at saturation ($\Delta\mu = 0$) as a function of the wall radius. The symbols correspond to the numerical DFT results. The dashed line shows the prediction according to Eq. (51), where $\gamma^{\text{SIA}}_{lg}(\infty) = 0.524\varepsilon/\sigma^2$ (see Table I). The dashed-dotted line corresponds to Eq. (51) where $\gamma^{\text{SKA}}_{lg}(\infty) = 1.060\varepsilon/\sigma^2$ is used instead of $\gamma^{\text{SIA}}_{lg}(\infty)$. The wall parameters are $\rho_w\varepsilon_w = 0.8\varepsilon/\sigma^3$ and $\sigma_w = 1.25\sigma$ at $k_BT = 0.7\varepsilon$.

$\Delta\mu = 0$ is crossed by the adsorption isotherm at large ℓ, in agreement with the result depicted in Fig. 9. However, for a *given* R, ℓ as obtained by SKA is underestimated, which follows from Eq. (51) with $\gamma_{lg}(\infty) = \gamma^{\text{SKA}}_{lg}(\infty)$, which is also consistent with the physical observation that high surface tension inhibits growth of the liquid film.

Note that these results are not in conflict with the previous study in Ref. [8], where the SKA has been applied for drying on a spherical hard wall and very good agreement was obtained with DFT computations. This is because in Ref. [8] the "exact" (i.e., obtained from DFT computations) liquid-vapor surface tension was implemented into SKA with a view to verify the correctness of its functional form. Here, we show that the coarse-grained effective Hamiltonian approach is capable of a quantitatively reliable prediction of the adsorption phenomena on a spherical wall (for a sufficiently large R), if the restriction of the sharp liquid-gas interface is dropped. However, the price we have to pay is one more parameter (compared to SKA) that steps into the theory.

V. SUMMARY AND CONCLUSIONS

We have reexamined the properties of a well known coarse-grained interfacial Hamiltonian approach, originally proposed by Dietrich [1] for the study of wetting phenomena on a planar substrate and based on SKA. SKA relies on approximating the density profile by a piecewise constant function and has proved to provide significant insight into interfacial phenomena as it is mathematically tractable and gives reliable results for a wide spectrum of problems. This theory is phenomenological in its origin, but a link with a microscopic DFT can be made, which allows one to express all the necessary quantities in terms of fluid-fluid and fluid-substrate interaction parameters. Comparison with numerical DFT reveals that SKA provides a

fully satisfactory approach to the theory of complete wetting on a planar surface.

One of the aims of this study was to demonstrate that for a spherical geometry the prediction quality of SKA regarding interfacial properties and wetting characteristics is limited. More specifically, we demonstrated that SKA satisfactorily determines the functional form of the asymptotic behavior of the film thickness for large radii of the substrate but leads to a significant quantitative disagreement in the prediction of the adsorbed film thickness when compared against numerical DFT. The source of the deviation is the presence of the Laplace pressure that is not quantitatively captured within the framework of SKA. This contribution originates in the dependence of the free energy of the liquid-gas interface on a position of a dividing surface, a property that is absent in the planar case.

We then showed that the properties of the effective interfacial Hamiltonian approach can be substantially improved if SKA is replaced by SIA, where the assumption of the sharp liquid-gas interface is replaced by a less restrictive approximation in which the interface is treated as a continuous function of the density distribution. We demonstrated that SIA allows for mathematical scrutiny as it is still analytically tractable, e.g., it provides the curvature expansion of the surface tensions (nonanalytic in the wall curvature) with the leading-order term proportional to σ/R. Moreover, it allows one to express the corresponding coefficient, the Tolman length, in a fairly simple manner and the values it predicts for the Tolman length are in reasonable agreement with the latest simulation results.

This is in contrast with SKA, where the linear term in the surface tension expansion is missing, i.e., the Tolman length vanishes. This observation is in full agreement with the conclusion of Fisher and Wortis [28], since SKA treats the fluid in a "symmetric" way, and thus the Tolman length must disappear as for the Ising-like models. In other words, according to SKA, the surface tension of a large drop is equivalent to the one of a bubble, provided the density profiles of the two systems are perfectly antisymmetric in the planar limit. This is no more true for SIA, due to the asymmetry of the "local" contributions to the surface tension, i.e., the first term on the right-hand side of Eq. (38).

Furthermore, comparison with our numerical DFT revealed that the SIA results of the film thickness as a function of the wall radius offer a significant improvement to the ones obtained from SKA. This follows from the fact that the surface tension of the planar liquid-gas interface according to SKA is overestimated, which in turn underestimates the interface growth.

It should be emphasized that all the theoretical approaches we have considered in this work are of a mean-field character, i.e., they do not properly take into account the interfacial fluctuations (capillary waves) at the liquid-gas interface. However, for our fluid model of a power-law interaction, these fluctuations are not expected to play any significant role, since the upper critical dimension associated with the considered system is $d_c^* = 2$ [34]. Nevertheless, what one has to take into account in order to obtain the correct critical behavior, is the broadening of the interface at the critical region. Evidently, this feature is not provided by SKA. Consequently, within

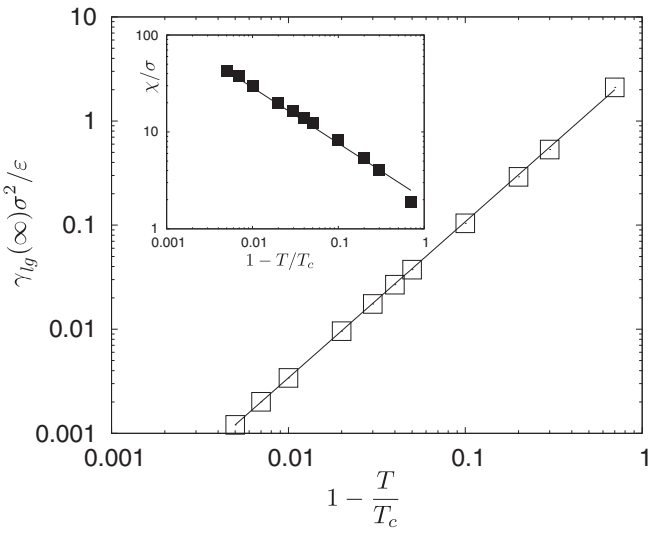

FIG. 11. Plot of liquid-gas surface tension vs $t = 1 - T/T_c$. The squares are the result of SIA, where a simple linear interpolant has been used to model the interface density profile. The surface tension has been obtained by minimizing the grand potential with respect to the interface width χ. The solid line is a fit to $\gamma_{lg}(\infty)\sigma^2/\varepsilon = Ct^{3/2}$, where the resulting coefficient is $C = 3.4$. The inset shows a plot of the interface width χ/σ over t. The solid line is a fit to $\chi = C_\chi t^{-\alpha}$, where $C_\chi = 2.0$ and $\alpha = 0.57$.

SKA the liquid-gas surface tension vanishes as $t = 1 - \frac{T}{T_c}$ [5]. In contrast, SIA provides the expected mean-field behavior $\gamma_{lg}(\infty) \sim t^{3/2}$, as it is able to capture the interface broadening near the critical point (see Fig. 11).

The SIA developed here can be naturally extended by "softening" the wall-liquid interface in an analogous way as done for the liquid-vapor interface. However, such a modification would have presumably only negligible impact on the prediction of the thickness of the adsorbed liquid film, since the contribution to the excess free energy from the wall-liquid surface tension has no ℓ dependence and the change of the binding potential is expected to be small. On the other hand, it may be interesting to find the influence of this refinement on quantities such as the density profile at contact with the wall. However, for this purpose a nonlocal DFT (e.g., Rosenfeld's fundamental measure theory) would be needed [8,35,36].

We also note that despite our restriction to a model of spherical symmetry, our conclusions should be relevant for general curved geometries and should capture some of the qualitative aspects of wetting on nonplanar substrates. Of particular interest would be the extension of this study to spatially heterogeneous, chemical, or topographical substrates. Such substrates have a significant effect on the wetting characteristics of the solid-liquid pair (e.g., Refs. [37–42]).

ACKNOWLEDGMENTS

We are grateful to Bob Evans for valuable comments and suggestions on an early version of the manuscript and for bringing to our attention Ref. [35]. We thank Antonio Pereira for helpful discussions regarding numerical aspects of our

study. This work is supported by the Rotary Clubs Darmstadt, Darmstadt-Bergstraße, and Darmstadt-Kranichstein, Engineering and Physical Sciences Research Council of England Platform Grant No. EP/E046029, European Union-FP7 ITN Grant No. 214919 (Multiflow) and European Research Council Advanced Grant No. 247031. A.M. is grateful for the financial support of the Ministry of Education, Youth and Sports of the Czech Republic under Project No. LC512 and the GAAS of the Czech Republic (Grant No. IAA400720710).

APPENDIX A: NUMERICAL METHODS

For our computations we employ dimensionless values. We use σ and ε as the characteristic length and energy scales, respectively.

1. Density profile

To obtain the equilibrium density profiles, the extremal conditions (9) and (13) for the planar and the spherical case, respectively, must be solved numerically. As both cases are of dimension one, the same numerical method can be applied and we restrict ourselves to presenting the numerical method for the planar wall, $W = \mathbb{R}^2 \times \mathbb{R}^-$.

The domain $\mathbb{R}$ normal to the wall is restricted to an interval of interest $[z_0, z_N]$ with boundary conditions $\rho(z) = 0$ for $z < z_0$ and $\rho(z) = \rho_g$ for $z > z_N$. $z_0 \in (0,1)$ is typically chosen to be 0.6. This can be done due to the repulsive character of the wall. The interval $[z_0, z_N]$ is then divided in a uniform mesh, $z_i = z_0 + i\Delta z$ with $i = 0, \ldots, N$, where $\Delta z = (z_N - z_0)/N$ is the grid size. Subsequently, the integral in Eq. (9) is discretized using a trapezoidal rule inside the domain $[z_0, z_N]$, whereas the analytical expression

$$\Psi_{\mathrm{Pla}}(z) = \int_z^\infty \Phi_{\mathrm{Pla}}(z')\,dz' = \begin{cases} \left(-\frac{16}{9}\pi + \frac{6}{5}\pi\frac{z}{\sigma}\right)\varepsilon\sigma^3, & \text{if } z < \sigma \\ 4\pi\varepsilon\sigma^3\left[\frac{1}{45}\left(\frac{\sigma}{z}\right)^9 - \frac{1}{6}\left(\frac{\sigma}{z}\right)^3\right], & \text{if } z \geqslant \sigma \end{cases}$$

is used for the integral outside that interval. Hence, we obtain a system of $N+1$ nonlinear equations with $\{\rho_i,\ i = 0, \ldots, N\}$ as unknowns, namely,

$$g_i(\rho_0, \ldots, \rho_N) := \mu_{\mathrm{HS}}(\rho_i) + V_\infty(z_i) - \mu + \rho_g \Psi_{\mathrm{Pla}}(z_N - z_i) + \frac{\Delta z}{2}\sum_{j=1}^{N-1}(2 - \delta_{j0} - \delta_{jN})\rho_j \Phi_{\mathrm{Pla}}(|z_j - z_i|) = 0, \qquad \text{(A1)}$$

where δ_{ij} denotes the Kroenecker delta, which we have used in order to take into account the grid size at the boundaries.

This system of equations is solved using a modified Newton method, where each step $\Delta\boldsymbol{\rho}$ is rescaled with a parameter λ such that $\boldsymbol{\rho}^{n+1} = \boldsymbol{\rho}^n + \lambda\Delta\boldsymbol{\rho}$ is bounded in $(0, 6/\pi)$ in order to avoid the singularity of Eq. (8). Note that we have made use of the vector notation $\boldsymbol{\rho} := (\rho_0, \ldots, \rho_n)^T$. In each Newton step n, the linear system of equations

$$\mathbf{J} \cdot \Delta\boldsymbol{\rho} = \mathbf{g}(\boldsymbol{\rho}^n) \qquad \text{(A2)}$$

has to be solved, where the elements of the Jacobian matrix $\mathbf{J}$ are given by

$$J_{ij} = \frac{\partial g_i}{\partial \rho_j} = \delta_{ij}\mu'_{\mathrm{HS}}(\rho_i) + \frac{\Delta z}{2}(2 - \delta_{j0} - \delta_{jN})\Phi_{\mathrm{Pla}}(|z_j - z_i|). \qquad \text{(A3)}$$

2. Adsorption isotherms

Solving Eq. (A1) will only give one density profile $\boldsymbol{\rho}$ for each chemical potential μ. However, in the case of a prewetting transition, there can be multiple solutions for the same chemical potential. From these solutions, only one is stable, whereas the other solutions are meta- or unstable (see also Sec. III A). In order to compute the full bifurcation diagram of the set of density profiles over the chemical potential, a pseudo arc-length continuation scheme is developed similar to the one employed by Salinger and Frink [43].

More specifically, we introduce an arc-length parametrization such that $(\mu(s), \boldsymbol{\rho}(s))$ with $s \in \mathbb{R}$ is a connected set of solutions of condition (A1), and where we have included the chemical potential μ as an additional variable:

$$\mathbf{g}(\mu, \boldsymbol{\rho}) \stackrel{!}{=} \mathbf{0}. \qquad \text{(A4)}$$

The main idea of the continuation scheme is to trace the set of solutions along the curve parametrized by s.

Assume that a point $(\mu^n, \boldsymbol{\rho}^n)$ at position s^n on the curve is given, where n is the step of the continuation scheme being solved for. First, the tangent vector $(\frac{d\mu}{ds}, \frac{d\boldsymbol{\rho}}{ds})$ at position s^n is computed. This is done by differentiating $\mathbf{g}(s) := \mathbf{g}(\mu(s), \boldsymbol{\rho}(s))$ with respect to s. From Eq. (A4), it is known that $\mathbf{g}$ is a constant equal to zero on the curve of solutions $[\mu(s), \boldsymbol{\rho}(s)]$. Hence, the differential $\frac{d\mathbf{g}}{ds}$ vanishes:

$$\frac{d\mathbf{g}}{ds} = \left(\frac{\partial \mathbf{g}}{\partial \mu} \quad \mathbf{J}\right) \cdot \begin{pmatrix} \frac{d\mu}{ds} \\ \frac{d\boldsymbol{\rho}}{ds} \end{pmatrix} = 0, \qquad \text{(A5)}$$

where $\mathbf{J}$ is the Jacobian as defined in Eq. (A3) and

$$\frac{\partial g_i}{\partial \mu} = -1 + \frac{d\rho_g}{d\mu}\Psi_{\mathrm{Pla}}(z_N - z_i). \qquad \text{(A6)}$$

The second term takes into account that ρ_g for the density at $z > z_N$ depends on the chemical potential. In our computations, we have approximated $\frac{\partial g_i}{\partial \mu}$ by -1. Equation (A5) is the defining equation for the tangent vector $(\mu_T^n, \boldsymbol{\rho}_T^n) = (\frac{d\mu}{ds}, \frac{d\boldsymbol{\rho}}{ds})$.

We remark that this homogeneous system of linear equations leaves one degree of freedom, as we only have $N+1$ equations, but $N+2$ variables, $(\mu_T, \boldsymbol{\rho}_T)$. An additional equation is then used to maintain the direction of the tangent vector on the curve of solutions:

$$\left(\mu_T^{n-1} \quad \left(\boldsymbol{\rho}_T^{n-1}\right)^T\right) \cdot \begin{pmatrix} \mu_T^n \\ \boldsymbol{\rho}_T^n \end{pmatrix} = 1,$$

where $(\mu_T^{n-1} \quad (\boldsymbol{\rho}_T^{n-1})^T)$ is the tangent vector of the previous iteration.

In a second step, an additional equation for a point at the step size θ away from $(\mu^n, \boldsymbol{\rho}^n)$ and in the direction of the tangent vector $(\mu_T^{n-1} \quad (\boldsymbol{\rho}_T^{n-1})^T)$ is set up. For this purpose we introduce a scalar product, which takes into account

the discretization of the density profile into N intervals of length Δz:

$$\langle(\mu_1,\boldsymbol{\rho}_1)|(\mu_2,\boldsymbol{\rho}_2)\rangle := \mu_1\mu_2 + \cdots + \frac{\Delta z}{2}\sum_{j=0}^{N}(2-\delta_{j0}-\delta_{jN})\rho_{1j}\rho_{2j}. \quad \text{(A7)}$$

The norm with respect to this scalar product is defined as

$$\|(\mu,\boldsymbol{\rho})\| := \langle(\mu,\boldsymbol{\rho})\,|\,(\mu,\boldsymbol{\rho})\rangle^{1/2}. \quad \text{(A8)}$$

The curve of solutions $(\mu(s),\boldsymbol{\rho}(s))$ is now parametrized by the arc length with respect to the norm given above, such that,

$$\int_{s^n}^{s^n+\theta}\left\|\left(\frac{d\mu}{ds},\frac{d\boldsymbol{\rho}}{ds}\right)\right\| ds = \theta. \quad \text{(A9)}$$

Linearizing the norm around s^n and making use of the approximate tangent vector $(\mu_T,\boldsymbol{\rho}_T)$ at s^n, one obtains

$$\left\langle\left(\mu_T^n,\boldsymbol{\rho}_T^n\right)\middle|\left(\mu(s^n+\theta)-\mu(s^n),\boldsymbol{\rho}(s^n+\theta)-\boldsymbol{\rho}(s^n)\right)\right\rangle = \theta, \quad \text{(A10)}$$

where we have made use of the normalized tangent vector such that

$$\|(\mu_T^n,\boldsymbol{\rho}_T^n)\| = 1. \quad \text{(A11)}$$

Inserting $(\mu^{n+1},\boldsymbol{\rho}^{n+1})$ for $(\mu(s^n+\theta),\boldsymbol{\rho}(s^n+\theta))$ into Eq. (A10) leads to the additional equation for the next point on the curve of solutions:

$$K_n(\mu^{n+1},\boldsymbol{\rho}^{n+1}) := \left\langle\left(\mu_T^n,\boldsymbol{\rho}_T^n\right)\middle|\left(\mu^{n+1}-\mu^n,\boldsymbol{\rho}^{n+1}-\boldsymbol{\rho}^n\right)\right\rangle - \theta \overset{!}{=} 0. \quad \text{(A12)}$$

For a geometric interpretation of Eq. (A12), see Fig. 12.

To obtain $(\mu^{n+1},\boldsymbol{\rho}^{n+1})$, Eq. (A12) is solved together with Eq. (A4). This is done using a Newton scheme. In each Newton step, the following system of linear equations is solved:

$$\begin{pmatrix}\mu_T^n & (\bar{\boldsymbol{\rho}}_T^n)^T\\ \frac{\partial\mathbf{g}}{\partial\mu} & \mathbf{J}\end{pmatrix}\cdot\begin{pmatrix}\Delta\mu^m\\ \Delta\boldsymbol{\rho}^m\end{pmatrix} = \begin{pmatrix}K_n(\mu^{n,m},\boldsymbol{\rho}^{n,m})\\ \mathbf{g}(\mu^{n,m},\boldsymbol{\rho}^{n,m})\end{pmatrix}, \quad \text{(A13)}$$

where we are considering the nth step of the continuation scheme and the mth step of the Newton method, such that

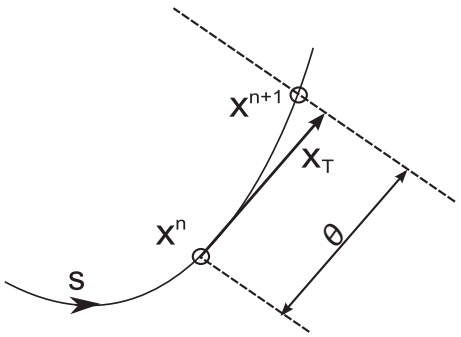

FIG. 12. Sketch of one iteration step of the continuation scheme. $\mathbf{x}^n$ and $\mathbf{x}^{n+1}$ are consecutive points of the iteration, where $\mathbf{x}=(\mu,\boldsymbol{\rho})$. $\mathbf{x}_T$ is the tangent vector at $\mathbf{x}^n$. By following the curve of solutions in the direction of the tangent vector, the pseudo arc-length continuation scheme is able to trace the curve of solutions through turning points with respect to the parameter μ.

$\Delta\mu^m := \mu^{n,m+1}-\mu^{n,m}$ and $\Delta\boldsymbol{\rho}^m := \boldsymbol{\rho}^{n,m+1}-\boldsymbol{\rho}^{n,m}$. Furthermore, we have made use of

$$\bar{\rho}_{T,j}^n := \frac{\Delta z}{2}(2-\delta_{j0}-\delta_{jN})\rho_{T,j}^n.$$

Finally, Eq. (A13) is solved using a conjugate gradient method, where the Jacobian (A3) of the system is approximated by introducing a cutoff of five molecular diameters for the intermolecular potential Φ_{Pla}.

APPENDIX B: SURFACE TENSION AND BINDING POTENTIAL IN SKA

1. Surface tension

According to Gibbsian thermodynamics, the surface tension is the free-energy cost to increase an interface by unit area, i.e., the excess free energy (excess grand potential for an open system) per unit area with respect to the corresponding uniform phases. Within SKA, the liquid-vapor surface tension can be obtained from Eq. (7), with

$$\rho(\mathbf{r}) = \begin{cases}\rho_A, & \mathbf{r}\in\mathbb{V}_A\\ \rho_B, & \mathbf{r}\in\mathbb{V}_B,\end{cases} \quad \text{(B1)}$$

where $\mathbb{V}_A\cap\mathbb{V}_B = 0$ and $\mathbb{V}_A\cup\mathbb{V}_B = \mathbb{R}^3$. The convenience of the expression for the excess grand potential as given by Eq. (7) becomes evident now, as for $\rho_A=\rho_l$, $\rho_B=\rho_g$, and no external field, only the second term in Eq. (7) matters. One then gets an immediate result for the liquid-gas surface tension,

$$\gamma_{lg}^{\text{SKA}} = \frac{\Omega_{\text{ex}}}{\mathcal{A}} = -\frac{(\rho_l-\rho_g)^2}{\mathcal{A}}I(\mathbb{V}_A,\mathbb{V}_B), \quad \text{(B2)}$$

where

$$I(\mathbb{V}_A,\mathbb{V}_B) \equiv \frac{1}{2}\int_{\mathbb{V}_A}\int_{\mathbb{V}_B}\phi(|\mathbf{r}_1-\mathbf{r}_2|)\,d\mathbf{r}_1\,d\mathbf{r}_2. \quad \text{(B3)}$$

For the surface tension of a planar interface we have $\mathbb{V}_A = \mathbb{V}_{z<0}$ and $\mathbb{V}_B = \mathbb{V}_{z\geqslant 0}$ such that

$$\frac{I(\mathbb{V}_{z<0},\mathbb{V}_{z\geqslant 0})}{\mathcal{A}} = \frac{1}{2}\int_{-\infty}^{0}\int_{0}^{\infty}\Phi_{\text{Pla}}(|z-z'|)\,dz'\,dz,$$

with Φ_{Pla} defined by Eq. (11). Thus, for the liquid-gas surface tension we obtain

$$\gamma_{lg}^{\text{SKA}}(\infty) = -\frac{\Delta\rho^2}{2}\int_{-\infty}^{0}\int_{0}^{\infty}\Phi_{\text{Pla}}(|z-z'|)\,dz'\,dz = \frac{3}{4}\pi\Delta\rho^2\varepsilon\sigma^4. \quad \text{(B4)}$$

In the case of a spherical symmetry, i.e., a drop of liquid of radius R, $\mathbb{V}_A = \{\mathbf{r}\in\mathbb{R}^3 : |\mathbf{r}| < R\}$ and $\mathbb{V}_B = \{\mathbf{r}\in\mathbb{R}^3 : |\mathbf{r}|\geqslant R\}$, the surface tension becomes

$$\begin{aligned}\gamma_{lg}^{\text{SKA}}(R) &= -\Delta\rho^2\frac{I(\mathbb{V}_{r<R},\mathbb{V}_{r\geqslant R})}{4\pi R^2}\\ &= -\frac{\Delta\rho^2}{2}\int_R^\infty\int_0^R\left(\frac{r}{R}\right)^2\Phi_{\text{Sph}}(r,r')\,dr'\,dr\\ &= -\frac{\Delta\rho^2}{2}\int_R^\infty\left(\frac{r}{R}\right)^2\Psi_R(r)\,dr\\ &= \gamma_{lg}(\infty)\left(1-\frac{2}{9}\frac{\ln(R/\sigma)}{(R/\sigma)^2}+O\left((\sigma/R)^2\right)\right), \quad \text{(B5)}\end{aligned}$$

where $\Delta\rho = \rho_l - \rho_g$ and $\Phi_{\rm Sph}(r,r') \equiv \int_{\partial B_{r'}} \phi(|\mathbf{r}-\mathbf{r}'|)d\mathbf{r}'$ can be advantageously expressed in terms of $\Phi_{\rm Pla}$:

$$\begin{aligned}
&\Phi_{\rm Sph}(r,r') \\
&= \int_0^{2\pi}\int_0^{\pi} \phi(|\mathbf{r}-\mathbf{r}'|) r'^2 \sin\vartheta'\, d\vartheta'\, d\varphi' \\
&= 2\pi r'^2 \int_0^{\pi} \phi(\sqrt{r^2 - 2rr'\cos\vartheta' + r'^2}) \sin\vartheta'\, d\vartheta' \\
&= \pi \frac{r'}{r} \int_{(r-r')^2}^{(r+r')^2} \phi(\sqrt{t})\, dt \\
&= \pi \frac{r'}{r} \left[\int_{(r-r')^2}^{\infty} \phi(\sqrt{t})\, dt - \int_{(r+r')^2}^{\infty} \phi(\sqrt{t})\, dt \right] \\
&= 2\pi \frac{r'}{r} \left[\int_0^{\infty} \phi(\sqrt{(r-r')^2 + u^2}) u\, du \right. \\
&\quad \left. - \int_0^{\infty} \phi(\sqrt{(r+r')^2 + u^2}) u\, du \right] \\
&= \frac{r'}{r} [\Phi_{\rm Pla}(|r-r'|) - \Phi_{\rm Pla}(|r+r'|)], \qquad \text{(B6)}
\end{aligned}$$

and for $r > R$,

$$\Psi_R(r) \equiv \int_0^R \Phi_{\rm Sph}(r,r')\, dr' = \frac{\pi\varepsilon\sigma^4}{3r} \begin{cases} \frac{\sigma^8}{30}\left[\frac{r+9R}{(r+R)^9} - \frac{r-9R}{(r-R)^9}\right] + \sigma^2\left[\frac{r-3R}{(r-R)^3} - \frac{r+3R}{(r+R)^3}\right], & R+\sigma < r \\ -\frac{26}{15}\frac{r}{\sigma} - \frac{9}{5\sigma^2}[R^2 - (r-\sigma)^2] + \frac{27}{10} + \frac{\sigma^8}{30}\frac{r+9R}{(r+R)^9} - \sigma^2\frac{r+3R}{(r+R)^3}, & r < R+\sigma. \end{cases} \qquad \text{(B7)}$$

Note that expression (B5) gives a vanishing Tolman's length.

2. Binding potential

The binding potential of a system possessing two interfaces is the surface free energy per unit area of the system minus the contribution due to the surface tensions of the two interfaces. It expresses an effective interaction between the interfaces induced by the attractive forces. If, analogously to the analysis above, we define three disjoint subspaces $\mathbb{V}_W$, $\mathbb{V}_A$, and $\mathbb{V}_B$, such that $\mathbb{V}_W \cup \mathbb{V}_A \cup \mathbb{V}_B = \mathbb{R}^3$, the density distribution of the wall-liquid-gas system within SKA is

$$\rho(\mathbf{r}) = \begin{cases} 0, & \mathbf{r} \in \mathbb{V}_W \\ \rho_l, & \mathbf{r} \in \mathbb{V}_A \\ \rho_g, & \mathbf{r} \in \mathbb{V}_B, \end{cases} \qquad \text{(B8)}$$

which when substituted into Eq. (7) gives for the excess grand potential:

$$\begin{aligned}
\Omega_{\rm ex} = & -\Delta\mu\Delta\rho V_A - {\rho_l}^2 I(\mathbb{V}_W,\mathbb{V}_A) - \rho_g^2 I(\mathbb{V}_W,\mathbb{V}_B) \\
& - (\Delta\rho)^2 I(\mathbb{V}_A,\mathbb{V}_B) + \int_{\mathbb{V}_A\cup\mathbb{V}_B} V(\mathbf{r})\rho(\mathbf{r})d\mathbf{r}. \qquad \text{(B9)}
\end{aligned}$$

We now rearrange the terms in Eq. (B9), such that

$$\frac{\Omega_{\rm ex}(\ell)}{\mathcal{A}} = -\Delta\mu\Delta\rho\frac{V_A}{\mathcal{A}} + \gamma_{wl}^{\rm SKA} + \frac{\mathcal{A}'}{\mathcal{A}}\gamma_{lg}^{\rm SKA} + w^{\rm SKA}(\ell), \qquad \text{(B10)}$$

where $\mathcal{A} = \int_{\partial\mathbb{V}_W} dS$ is the surface of the wall and $\mathcal{A}' = \int_{\partial(\mathbb{V}_W\cup\mathbb{V}_A)} dS$ is the surface of the liquid-gas interface. We obtain

$$\gamma_{wl}^{\rm SKA} = \frac{1}{\mathcal{A}}\left(-{\rho_l}^2 I(\mathbb{V}_W,\mathbb{V}_A\cup\mathbb{V}_B) + \rho_l\int_{\mathbb{V}_A\cup\mathbb{V}_B} V(\mathbf{r})\, d\mathbf{r}\right), \qquad \text{(B11)}$$

$$\gamma_{lg}^{\rm SKA} = -\frac{1}{\mathcal{A}'}(\Delta\rho)^2 I(\mathbb{V}_W\cup\mathbb{V}_A,\mathbb{V}_B), \qquad \text{(B12)}$$

and the binding potential $w^{\rm SKA}$ involving the remaining contribution

$$w^{\rm SKA}(\ell) = \frac{1}{\mathcal{A}}\left(2\rho_l\Delta\rho I(\mathbb{V}_W,\mathbb{V}_B) - \Delta\rho\int_{\mathbb{V}_B} V(\mathbf{r})\, d\mathbf{r}\right). \qquad \text{(B13)}$$

Having obtained the expressions of $I(X,Y)$ for systems possessing translational or spherical symmetry, we can evaluate the binding potential in the planar case by making use of $\mathbb{V}_w = \mathbb{R}^2\times(-\infty,\delta]$, $\mathbb{V}_A = \mathbb{R}^2\times(\delta,\ell)$ and $\mathbb{V}_B = \mathbb{R}^2\times[\ell,\infty)$:

$$\begin{aligned}
&w^{\rm SKA}(\ell) \\
&\overset{\rm plane}{=} \Delta\rho\left(\rho_l\int_{\ell-\delta}^{\infty}\int_z^{\infty}\Phi_{\rm Pla}(z')\, dz'\, dz - \int_{\ell}^{\infty} V_{\infty}(z)\, dz\right) \\
&= -\frac{A}{12\pi\ell^2}\left(1 + \frac{2+3\frac{\delta}{\ell}}{1-\frac{\rho_w\varepsilon_w\sigma_w^6}{\rho_l^2\varepsilon\sigma^6}}\frac{\delta}{\ell} + O\big((\delta/\ell)^3\big)\right). \qquad \text{(B14)}
\end{aligned}$$

In the spherical case we make use of $\mathbb{V}_w = \{\mathbf{r}\in\mathbb{R}^3 : |\mathbf{r}| \leqslant R+\delta\}$, $\mathbb{V}_A = \{\mathbf{r}\in\mathbb{R}^3 : R+\delta < |\mathbf{r}| < R+\ell\}$, and $\mathbb{V}_B = \{\mathbf{r}\in\mathbb{R}^3 : |\mathbf{r}| \geqslant R+\ell\}$ to obtain

$$w^{\rm SKA}(\ell;R) \overset{\rm sphere}{=} w^{\rm SKA}(\ell;\infty)\left(1 + \frac{\ell}{R}\right), \qquad \text{(B15)}$$

where we have neglected terms $O\big((\delta/\ell)^3, \delta/R, \frac{\ln(\ell/R)}{(R/\ell)^2}\big)$.

APPENDIX C: SURFACE TENSION, BINDING POTENTIAL, AND THE TOLMAN LENGTH IN SIA

1. Surface tension

The surface tension of a planar liquid-gas interface in SIA

$$\rho_{lg,\infty}(z) = \begin{cases} \rho_l, & z \leqslant -\chi/2 \\ \rho_{lg}(z), & |z| < \chi/2 \\ \rho_g, & z \geqslant \chi/2, \end{cases} \qquad \text{(C1)}$$

is obtained by substituting Eq. (C1) into Eq. (7) with $V(\mathbf{r}) = 0$,

$$\begin{aligned}\gamma_{lg}^{\mathrm{SIA}}(\infty) &= \frac{\Omega_{\mathrm{ex}}[\rho_{lg,\infty}]}{\mathcal{A}} \\ &= -\int_{-\chi/2}^{\chi/2}\{p[\rho_{lg,\infty}(z)] - p[\rho_{\mathrm{ref}}(z)]\}dz \\ &\quad + \frac{1}{2}\int_{-\infty}^{\infty}\int_{-\infty}^{\infty}\rho_{lg,\infty}(z)[\rho_{lg,\infty}(z') - \rho_{lg,\infty}(z)] \\ &\quad \times \Phi_{\mathrm{Pla}}(z,z')dz'\,dz, \end{aligned} \tag{C2}$$

where $\rho_{\mathrm{ref}}(z)$ denotes the density of a given bulk phase, i.e., $\rho_{\mathrm{ref}}(z) = \rho_l\Theta(-z) + \rho_g\Theta(z)$ such that at saturation $p[\rho_{\mathrm{ref}}(z)] \equiv p_{\mathrm{ref}} = \mathrm{const}$. We note that in the above approximation the contribution due to the excess local pressure is generally nonzero (in contrast to SKA).

In the spherical case, the density profile is

$$\rho_{lg,R}(r) = \begin{cases}\rho_{l,} & r \leqslant R - \chi/2 \\ \rho_{lg}(r-R), & |r-R| < \chi/2 \\ \rho_{g,} & r \geqslant R + \chi/2,\end{cases} \tag{C3}$$

and the surface tension of a liquid drop of radius R is

$$\begin{aligned}\gamma_{lg}^{\mathrm{SIA}}(R) &= \frac{\Omega_{\mathrm{ex}}[\rho_{lg,R}]}{4\pi R^2} \\ &= -\int_{R-\chi/2}^{R+\chi/2}\{p[\rho_{lg,R}(r)] - p_{\mathrm{ref}}\}\left(\frac{r}{R}\right)^2 dr \\ &\quad + \frac{1}{2}\int_0^{\infty}\int_0^{\infty}\rho_{lg,R}(r)[\rho_{lg,R}(r') - \rho_{lg,R}(r)] \\ &\quad \times \Phi_{\mathrm{Sph}}(r,r')\left(\frac{r}{R}\right)^2 dr'\,dr. \end{aligned} \tag{C4}$$

2. Tolman length

Here we calculate the Tolman length as given by SIA by a direct comparison of Eqs. (C2) and (C4). We first compare the second terms of Eqs. (C2) and (C4). For this purpose we define

$$\begin{aligned} h_R(r,r') &\equiv \rho_{lg,R}(r)[\rho_{lg,R}(r') - \rho_{lg,R}(r)] \\ \text{and}\quad h(r,r') &\equiv \rho_{lg,\infty}(r)[\rho_{lg,\infty}(r') - \rho_{lg,\infty}(r)], \end{aligned} \tag{C5}$$

and making use of Eq. (B6) we can express the double integral in Eq. (C4) as

$$\begin{aligned}&\frac{\sigma^2}{\varepsilon}\int_0^{\infty}\int_0^{\infty}h_R(r,r')\Phi_{\mathrm{Sph}}(r,r')\left(\frac{r}{R}\right)^2 dr'\,dr \\ &= \frac{\sigma^2}{\varepsilon}\int_{-R}^{\infty}\int_{-R}^{\infty}h(r,r')[\Phi_{\mathrm{Pla}}(|r-r'|) \\ &\quad -\Phi_{\mathrm{Pla}}(|2R + r - r'|)]\left(1 + \frac{r'}{R}\right)\left(1 + \frac{r}{R}\right)dr'\,dr \\ &= \frac{\sigma^2}{\varepsilon}\int_{-R}^{\infty}\int_{-R}^{\infty}h(r,r')\Phi_{\mathrm{Pla}}(|r-r'|) \\ &\quad \times\left(1 + \frac{r'}{R}\right)\left(1 + \frac{r}{R}\right)dr'\,dr + O\big((\sigma/R)^2\big) \\ &= \frac{\sigma^2}{\varepsilon}\int_{-R}^{\infty}\int_{-R}^{\infty}h(r,r')\Phi_{\mathrm{Pla}}(|r-r'|) \\ &\quad \times\left(1 + \frac{r+r'}{R}\right)dr'\,dr + O\left(\frac{\ln(R/\sigma)}{(R/\sigma)^2}\right) \\ &= \frac{\sigma^2}{\varepsilon}\int_{-\infty}^{\infty}\int_{-\infty}^{\infty}h(r,r')\Phi_{\mathrm{Pla}}(|r-r'|) \\ &\quad \times\left(1 + \frac{r+r'}{R}\right)dr'\,dr + O\left(\frac{\ln(R/\sigma)}{(R/\sigma)^2}\right). \end{aligned} \tag{C6}$$

Comparison with the double integral in Eq. (C2) then yields

$$\begin{aligned}&\frac{\sigma^2}{\varepsilon R}\iint_{-\infty}^{\infty}h(r,r')\Phi_{\mathrm{Pla}}(|r-r'|)(r+r')\,dr'\,dr \\ &\quad + O\left(\frac{\ln(R/\sigma)}{(R/\sigma)^2}\right) \\ &= \frac{\sigma^2}{\varepsilon R}\int_{-\infty}^{\infty}\int_{-\infty}^{\infty}r[h(r,r') + h(r',r)]\Phi_{\mathrm{Pla}}(|r-r'|)\,dr'\,dr \\ &\quad + O\left(\frac{\ln(R/\sigma)}{(R/\sigma)^2}\right) \\ &= -\frac{\sigma^2}{\varepsilon R}\int_{-\infty}^{\infty}\int_{-\infty}^{\infty}r[\rho_{lg,\infty}(r') - \rho_{lg,\infty}(r)]^2 \\ &\quad \times\Phi_{\mathrm{Pla}}(|r-r'|)dr'\,dr + O\left(\frac{\ln(R/\sigma)}{(R/\sigma)^2}\right). \end{aligned}$$

In the following, we focus on the asymmetry of the model due to the contribution of the pressure, but for simplicity we assume that the density profile is symmetric. In this case, the integrand in the above expression is antisymmetric with respect to the reflection transformation $r \to -r$ and $r' \to -r'$ and the term $O(\sigma/R)$ vanishes.

For the difference of the first terms of Eqs. (C4) and (C2) we obtain

$$\begin{aligned}&-\frac{\sigma^2}{\varepsilon}\int_0^{\infty}\{p[\rho_{lg,R}(r)] - p_{\mathrm{ref}}\}\left(\frac{r}{R}\right)^2 dr \\ &\quad + \frac{\sigma^2}{\varepsilon}\int_{-\infty}^{\infty}\{p[\rho_{lg,\infty}(z)] - p_{\mathrm{ref}}\}\,dz \\ &= -\frac{2\sigma^2}{\varepsilon R}\int_{-\chi/2}^{\chi/2}\{p[\rho_{lg,\infty}(z)] - p_{\mathrm{ref}}\}z\,dz \\ &\quad + O\big((\sigma/R)^2\big), \end{aligned} \tag{C7}$$

yielding a Tolman length

$$\delta_{\infty} = \frac{1}{\gamma_{lg}^{\mathrm{SIA}}(\infty)}\int_{-\chi/2}^{\chi/2}\{p[\rho_{lg}(z)] - p_{\mathrm{ref}}\}z\,dz. \tag{C8}$$

Note that in line with [28], the Tolman length does not depend on the choice of the dividing surface.

3. Binding potential

The extension of the expression for the binding potential, Eq. (B15), as given by SKA is rather straightforward. We consider the density distribution as follows:

$$\rho(\mathbf{r}) = \begin{cases}0, & \mathbf{r} \in \mathbb{V}_W \\ \rho_l, & \mathbf{r} \in \mathbb{V}_A \\ \rho_{lg}(\mathbf{r}), & \mathbf{r} \in \mathbb{V}_{AB} \\ \rho_g, & \mathbf{r} \in \mathbb{V}_B,\end{cases} \tag{C9}$$

for $\mathbb{V}_W$ a sphere of radius $R+\delta$, for $\mathbb{V}_W \cup \mathbb{V}_A$ a sphere of radius $R+\ell-\chi/2$, and for $\mathbb{V}_W \cup \mathbb{V}_A \cup \mathbb{V}_{AB}$ a sphere of radius $R+\ell+\chi/2$ and $\mathbb{V}_W \cup \mathbb{V}_A \cup \mathbb{V}_B \cup \mathbb{V}_{AB} = \mathbb{R}^3$. Such a model is relevant for the study of wetting on a spherical (R finite) and on a planar ($R \to \infty$) wall. It should be noted that in contrast to SKA, this density distribution is not piecewise constant, due to the position dependent part of $\rho(\mathbf{r})$ in the region $\mathbb{V}_{AB}$. Furthermore, we define the following operators:

$$[XY] \equiv -\frac{1}{2}\int_X\int_Y [\rho(\mathbf{r})-\rho(\mathbf{r}')]^2\phi(|\mathbf{r}-\mathbf{r}'|)\,d\mathbf{r}'\,d\mathbf{r},$$
$$[XY]_{wl} \equiv -\frac{1}{2}\int_X\int_Y [\rho_{wl}(\mathbf{r})-\rho_{wl}(\mathbf{r}')]^2\phi(|\mathbf{r}-\mathbf{r}'|)\,d\mathbf{r}'\,d\mathbf{r},$$
$$[XY]_{lg} \equiv -\frac{1}{2}\int_X\int_Y [\rho_{lg}(\mathbf{r})-\rho_{lg}(\mathbf{r}')]^2\phi(|\mathbf{r}-\mathbf{r}'|)\,d\mathbf{r}'\,d\mathbf{r},$$

with $\rho_{wl}(\mathbf{r}) \equiv \rho_l \chi_{\mathbb{R}^3\setminus\mathbb{V}_W}(\mathbf{r})$ and $\rho_{lg}(\mathbf{r}) \equiv \rho_l \chi_{\mathbb{V}_W\cup\mathbb{V}_A}(\mathbf{r}) + \rho_{lg}(\mathbf{r})\chi_{\mathbb{V}_{AB}}(\mathbf{r}) + \rho_g \chi_{\mathbb{V}_B}(\mathbf{r})$, where $\chi_X(\mathbf{r})$ is the characteristic function of a subset X. Using this convention, the wall-liquid and liquid-gas surface tensions can be respectively expressed as

$$\gamma_{wl} = \frac{1}{\mathcal{A}}\left([\mathbb{V}_W\mathbb{V}_A] + [\mathbb{V}_W(\mathbb{V}_{AB}\cup\mathbb{V}_B)]_{wl} + \int \rho_{wl}(\mathbf{r})V(\mathbf{r})d\mathbf{r}\right)$$
$$\gamma_{lg} = \frac{1}{\mathcal{A}}\left([\mathbb{V}_{AB}\mathbb{V}_B] + \frac{1}{2}[\mathbb{V}_{AB}\mathbb{V}_{AB}] + [\mathbb{V}_A(\mathbb{V}_{AB}\cup\mathbb{V}_B)]\right.$$
$$\left. + [\mathbb{V}_W(\mathbb{V}_{AB}\cup\mathbb{V}_B)]_{lg} - \int_{\mathbb{V}_{AB}} \{p[\rho_{lg}(\mathbf{r})] - p_{\text{ref}}\}\,d\mathbf{r}\right),$$

where $\mathcal{A} = 4\pi R^2$. When this is subtracted from the surface grand potential (7), which can be written as

$$\frac{\Omega_{\text{ex}}}{\mathcal{A}} = \frac{1}{\mathcal{A}}\left([\mathbb{V}_W\mathbb{V}_A] + [\mathbb{V}_W(\mathbb{V}_{AB}\cup\mathbb{V}_B)]\right.$$
$$+ [\mathbb{V}_A(\mathbb{V}_{AB}\cup\mathbb{V}_B)] + \frac{1}{2}[\mathbb{V}_{AB}\mathbb{V}_{AB}] + [\mathbb{V}_{AB}\mathbb{V}_B]$$
$$\left. - \int_{\mathbb{V}_{AB}} \{p[\rho_{lg}(\mathbf{r})] - p[\rho_{\text{ref}}(\mathbf{r})]\}\,d\mathbf{r} + \int \rho(\mathbf{r})V(\mathbf{r})\,d\mathbf{r}\right), \tag{C10}$$

one obtains for the binding potential:

$$w^{\text{SIA}} = \frac{1}{\mathcal{A}}\left([\mathbb{V}_W(\mathbb{V}_{AB}\cup\mathbb{V}_B)] - [\mathbb{V}_W(\mathbb{V}_{AB}\cup\mathbb{V}_B)]_{wl}\right.$$
$$\left. - [\mathbb{V}_W(\mathbb{V}_{AB}\cup\mathbb{V}_B)]_{lg} + \int V(\mathbf{r})[\rho(\mathbf{r}) - \rho_{wl}(\mathbf{r})\,d\mathbf{r}]\right).$$

In spherical coordinates, the binding potential reads

$$w^{\text{SIA}} = \int_0^{R+\delta}\int_{R+\ell-\chi/2}^{\infty}\left(\frac{r}{R}\right)^2 \rho_l[\rho_l - \rho(r')]$$
$$\times\Phi_{\text{Sph}}(r,r')dr'\,dr$$
$$+ \int_{R+\ell-\chi/2}^{\infty}[\rho(r)-\rho_l]\,V_R(r)\left(\frac{r}{R}\right)^2 dr. \tag{C11}$$

[1] S. Dietrich, in *Phase Transitions and Critical Phenomena*, edited by C. Domb and J. L. Lebowitz (Academic, New York, 1988), Chap. 1, p. 2.
[2] D. Bonn, J. Eggers, J. Indekeu, J. Meunier, and E. Rolley, Rev. Mod. Phys. **81**, 739 (2009).
[3] M. Schick, in *Liquids at Interfaces*, Les Houches Session XLVIII, edited by J. Charvolin, J.-F. Joanny, and J. Zinn-Justin (Elsevier, Amsterdam, 1990).
[4] D. E. Sullivan and M. M. T. da Gama, *Fluid Interfacial Phenomena*, edited by C. A. Croxton (Wiley, New York, 1986), p. 45.
[5] T. Bieker and S. Dietrich, Physica A **252**, 85 (1998).
[6] R. Hołyst and A. Poniewierski, Phys. Rev. B **36**, 5628 (1987).
[7] R. Evans, J. R. Henderson, and R. Roth, J. Chem. Phys. **121**, 12074 (2004).
[8] M. C. Stewart and R. Evans, Phys. Rev. E **71**, 011602 (2005).
[9] J. R. Henderson, *Fundamentals of Inhomogeneous Fluids*, edited by D. Henderson (Dekker, New York, 1992).
[10] M. Napiórkowski and S. Dietrich, Phys. Rev. B **34**, 6469 (1986).
[11] N. D. Mermin, Phys. Rev. **137**, A1441 (1965).
[12] R. Evans, Adv. Phys. **28**, 143 (1979).
[13] J. A. Barker and D. Henderson, J. Chem. Phys. **47**, 4714 (1967).
[14] G. J. Throop and R. J. Bearman, J. Chem. Phys. **42**, 2408 (1965).
[15] S. Toxvaerd, J. Chem. Phys. **55**, 3116 (1971).
[16] J. K. Lee and L. A. Barker, J. Chem. Phys. **60**, 1976 (1974).
[17] E. A. Guggenheim, J. Chem. Phys. **13**, 253 (1945).
[18] R. Pandit, M. Schick, and M. Wortis, Phys. Rev. B **26**, 5112 (1982).
[19] E. H. Hauge and M. Schick, Phys. Rev. B **27**, 4288 (1983).
[20] M. Schick and P. Taborek, Phys. Rev. B **46**, 7312 (1992).
[21] D. Bonn and D. Ross, Rep. Prog. Phys. **64**, 1085 (2001).
[22] H. Kellay, J. Meunier, and B. P. Binks, Phys. Rev. Lett. **69**, 1220 (1992).
[23] G. Mistura, H. Lee, and M. Chan, J. Low Temp. Phys. **96**, 221 (1994).
[24] J. E. Rutledge and P. Taborek, Phys. Rev. Lett. **69**, 937 (1992).
[25] D. Ross, J. A. Phillips, J. E. Rutledge, and P. Taborek, J. Low Temp. Phys. **106**, 81 (1997).
[26] A. O. Parry, C. Rascon, and L. Morgan, J. Chem. Phys. **124**, 151101 (2006).
[27] R. C. Tolman, J. Chem. Phys. **17**, 333 (1948).
[28] M. P. A. Fisher and M. Wortis, Phys. Rev. B **29**, 6252 (1984).
[29] J. G. Sampayo, A. Malijevský, E. A. Müller, E. de Miguel, and G. Jackson, J. Chem. Phys. **132**, 141101 (2010).
[30] B. J. Block, S. K. Das, M. Oettel, P. Virnau, and K. Binder, J. Chem. Phys. **133**, 154702 (2010).
[31] A. E. van Giessen and E. M. Blokhuis, J. Chem. Phys. **131**, 164705 (2009).
[32] L. S. Bartell, J. Chem. Phys. B **105**, 11615 (2001).
[33] E. M. Blokhuis and J. Kuipers, J. Chem. Phys. **124**, 074701 (2006).

[34] R. Lipowsky, Phys. Rev. Lett. **52**, 1429 (1984).
[35] M. C. Stewart and R. Evans, J. Phys.: Condens. Matter **17**, S3499 (2005).
[36] E. M. Blokhuis and J. Kuipers, J. Chem. Phys. **126**, 054702 (2007).
[37] L. W. Schwartz and R. R. Elley, J. Colloid Interface Sci. **202**, 173 (1998).
[38] C. M. Gramlich, A. Mazouchi, and G. M. Homsy, Phys. Fluids **16**, 1660 (2004).
[39] D. Quéré, in *Thin Films of Soft Matter*, edited by S. Kalliadasis and U. Thiele (Springer Wien, New York, 2007), p. 115.
[40] N. Savva and S. Kalliadasis, Phys. Fluids **21**, 092192 (2009).
[41] N. Savva, S. Kalliadasis, and G. A. Pavliotis, Phys. Rev. Lett. **104**, 084501 (2010).
[42] H. Bohlen, A. O. Parry, E. Díaz-Herrera, and M. Schoen, Eur. Phys. J. E **25**, 103 (2008).
[43] A. G. Salinger and L. J. D. Frink, J. Chem. Phys. **118**, 7457 (2003).